LA-3676-MS

C.#3

LOS ALAMOS SCIENTIFIC LABORATORY
of the
University of California
LOS ALAMOS • NEW MEXICO

The ^{233}U Fission and Capture Cross Sections and Their Analysis at Low Energies

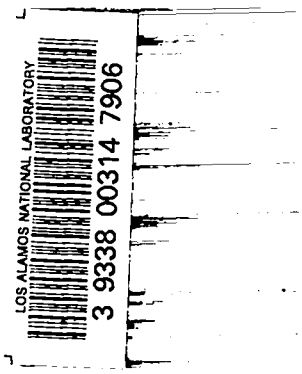

UNITED STATES
ATOMIC ENERGY COMMISSION
CONTRACT W-7405-ENG. 36

All LA...MS reports are informal documents, usually prepared for a special purpose and primarily prepared for use within the Laboratory rather than for general distribution. This report has not been edited, reviewed, or verified for accuracy. All LA...MS reports express the views of the authors as of the time they were written and do not necessarily reflect the opinions of the Los Alamos Scientific Laboratory or the final opinion of the authors on the subject.

Printed in the United States of America. Available from
Clearinghouse for Federal Scientific and Technical Information
National Bureau of Standards, U. S. Department of Commerce
Springfield, Virginia 22151
Price: Printed Copy $3.00; Microfiche $0.65

LA-3676-MS
UC-34, PHYSICS
TID-4500

LOS ALAMOS SCIENTIFIC LABORATORY
of the
University of California
LOS ALAMOS • NEW MEXICO

Report written: December 1966
Report distributed: May 4, 1967

The ^{233}U Fission and Capture Cross Sections and Their Analysis at Low Energies*

by

Delmar W. Bergen

*Also submitted as a thesis in partial fulfillment of the requirements for the degree of Doctor of Philosophy in Physics from the University of New Mexico.

ABSTRACT

The ^{233}U fission and capture cross sections were measured using a nuclear-device neutron source and time-of-flight techniques. Cross section data are presented from 20 to 10^6 eV for fission and from 20 to 63 eV for fission + capture.

The resonance region (20 eV to 63 eV) was fitted with both a single level function consisting of a sum of Breit-Wigner levels and the Reich and Moore* multilevel function based on R matrix theory. The resulting resonance parameters are listed and discussed.

In order to establish the validity of the resonance parameters derived from the multilevel fit, a study is presented of the cross section derived from two and three hypothetical resonances under various conditions and of the cross sections obtained from randomly generated resonances.

*C. W. Reich and M. S. Moore, Phys. Rev. 111, 929 (1958).

ACKNOWLEDGEMENTS

I would like to thank those in Groups P-3 and W-8 who have contributed to the time-of-flight experiments, especially Arthur Hemmendinger for directing this research, P. A. Seeger for his major effort in data reduction, Nancy Browne for assistance in figure preparation, Alita Roach for typing and proofreading the manuscript, and the Idaho Nuclear Corp.'s nuclear cross section group for providing the Reich-Moore multilevel code.

I also wish to express my appreciation to the Los Alamos Scientific Laboratory and the United States Atomic Energy Commission for supporting this research which formed the basis of a dissertation submitted to the University of New Mexico in partial fulfillment of the requirements for the degree of Doctor of Philosophy in Physics.

TABLE OF CONTENTS

LIST OF ILLUSTRATIONS

Figure

LIST OF TABLES

INTRODUCTION

For many years the idea of using the neutrons released in a nuclear explosion as a source for neutron physics experiments has been attractive, because of the incomparably great source strength, but formidable, because of the difficult working conditions associated with the release of a large amount of energy. In recent years, techniques have been developed for observing nuclear explosions emplaced in deep holes, with closures to contain all products of the explosion, a vacuum pipe providing a neutron flight path to ground surface, and a high degree of collimation of the neutron beam. Several preliminary tests have been performed in developing the special instrumentation required for using such neutrons with time-of-flight energy resolution to investigate the neutron interaction with nuclei and in June 1965 neutrons from a nuclear device were used successfully for measuring the neutron cross sections of several nuclei.[1-8] This report concerns itself with one of these, ^{233}U, on which both fission and capture cross sections were measured. The rather fascinating results, due to the good energy resolution and extremely low background, permitted a resonance analysis to be carried out over the energy interval 20 eV to 63 eV. Earlier studies[9] of ^{233}U have suggested that the fission of this nuclide is a several channel process and that interference effects are weak. Lynn[10] on the other hand has argued that for ^{233}U, whose average resonance spacing is only about twice the average resonance width,

the cross section shape will be dominated by level inteference. These ideas are investigated in some detail, and the interpretation of the cross section measurements in terms of single level and multilevel analyses of the data are presented.

I. DESCRIPTION OF THE EXPERIMENT

A. Experimental Layout

The neutron experiment, code named Petrel, was performed on June 11, 1965 at the Nevada Test Site. A schematic diagram of the experimental configuration is shown in Fig. 1. The neutron source, a nuclear device with a neutron yield of about 1.8×10^{23} neutrons within 0.1 μsec, was placed approximately 185 m below ground level. A vacuum pipe 35 cm in diameter provided a neutron flight path to ground surface. Immediately above the device there was a lead-polyethylene moderator, used to enhance the neutron flux at low energies. Anti-scattering baffles were located at intervals up the pipe, and near ground level a 122 cm long collimator formed a pencil beam of neutrons 1.9 cm in diameter. Neutrons passing through the collimator entered the experimental station containing a stack of seven fission foils, a ^{6}Li foil, background (Pt) foil, and three neutron-thick capture foils, as shown in Fig. 2. (The flight paths listed on the figure are distances from the moderator surface.) All foils were placed at 45^{o} angles to the beam; the fission foils were viewed by solid state detectors placed at 90^{o} and 55^{o}/or 125^{o} with respect to the beam, on a 90^{o} cone whose apex and axis coincided with the center and axis of the foil disk. The detectors, 5 cm from the foil center, were not exposed to the neutron beam. The geometry for all foils was as nearly identical as possible; the 90^{o} detector areas were 1 cm^2, presenting a solid angle of 0.04 sr; the $55^{o}/125^{o}$ detector areas were 3 cm^2, presenting a solid angle of 0.12 sr.

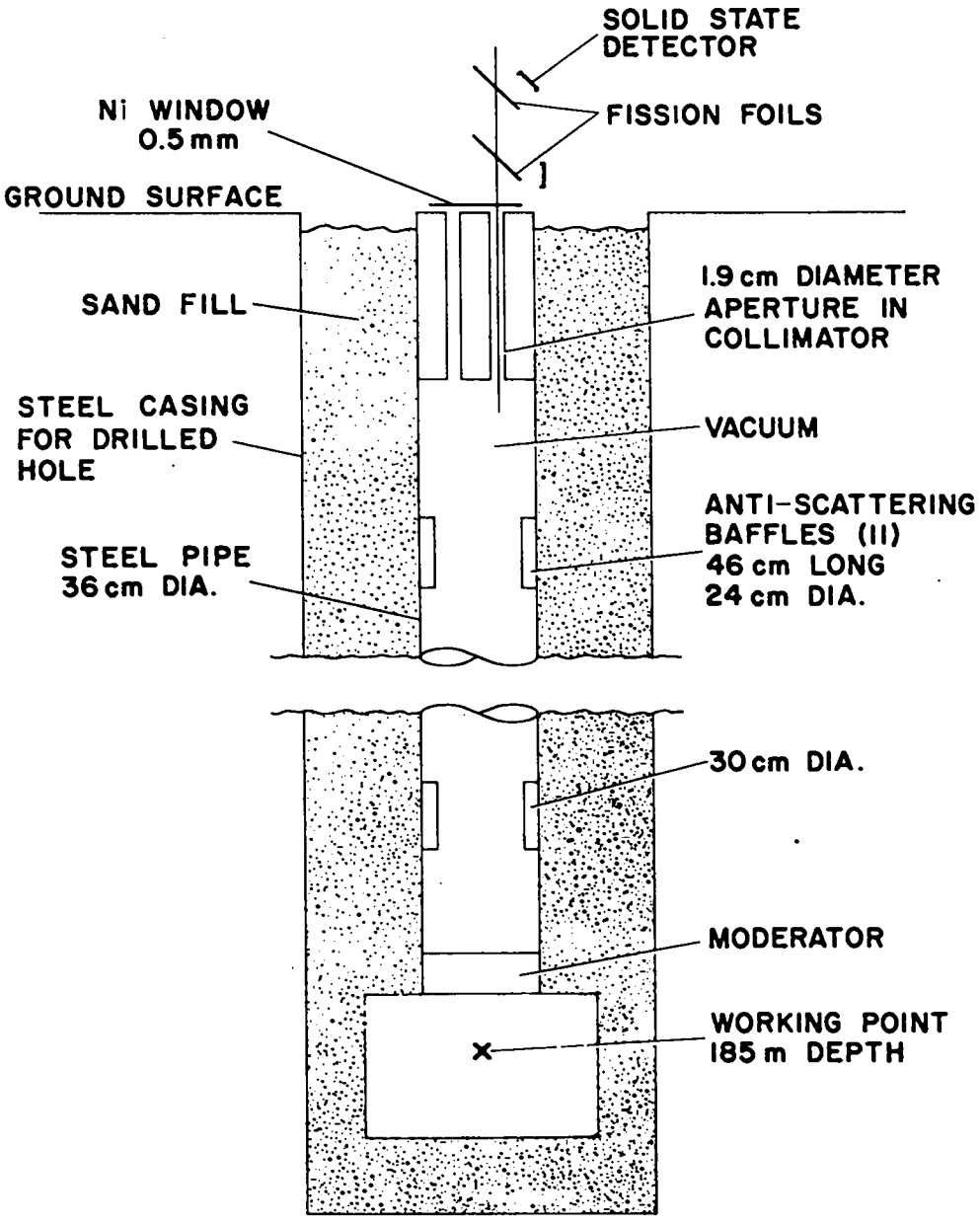

Fig. 1. General schematic diagram of the Petrel experimental layout.

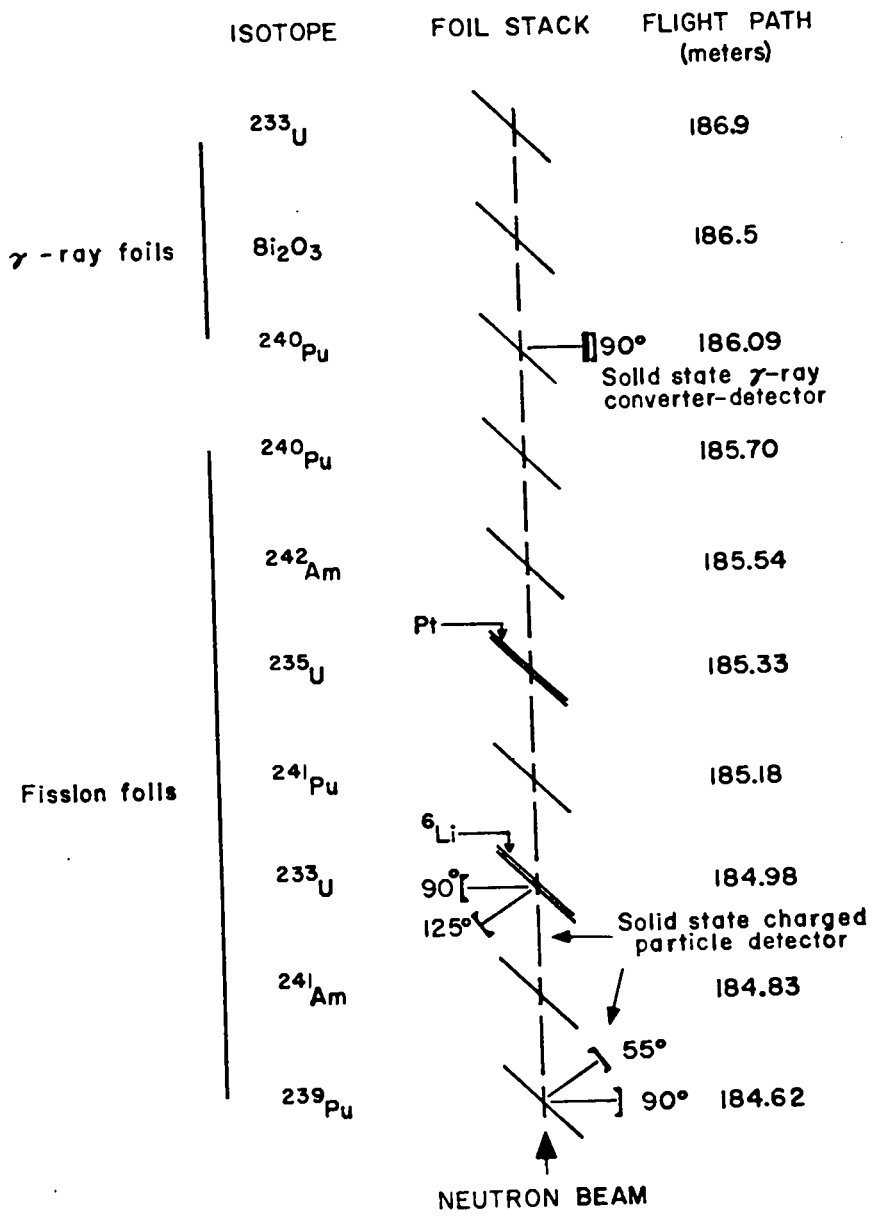

Fig. 2. Schematic diagram of the Petrel foil stack.

The capture foils, also placed at 45° to the beam, were viewed by Moxon-Rae type[11] γ-ray detectors placed 5 cm from the foil at 90° to the beam.

B. Data Recording

The fission foils were selected to be thin to both fission fragments and neutrons, yet dense enough to produce an average of 10^5 fission events per electronic resolution time (0.1 μsec). The 55°/125° detectors (0.12 sr solid angle) thus recorded an average of about 10^3 events per resolution time. At such rates, single events could not be observed; rather, the ionization in each detector, caused by the fission fragments, produced a current which was converted to a voltage across a resistor. This voltage was then logarithmically amplified and applied to the deflection plate of an oscilloscope. Logarithmic amplification was required to maintain accuracy over the dynamic range of the signal (as much as four decades). Each amplifier output was displayed on two oscilloscopes: a "raster" used for high resolution early time recording (0.1 μsec), and a "streak" for late time, low resolution recording (1 μsec). The electronic resolution of the system was about 0.1 μsec; therefore, a simple 1 μsec LRC smoother was placed on the input of the low resolution oscilloscope to reduce the effect of statistical fluctuations. Permanent records of the detector signals as a function of time were obtained by photographing the oscilloscopes with General Radio 35 mm moving-film cameras, Type 651. A simplified electronic schematic is shown in Fig. 3.

Figure 4 displays a typical film record for the streak mode. In this mode the oscilloscope beam was displaced at right angles to the film motion. Six data

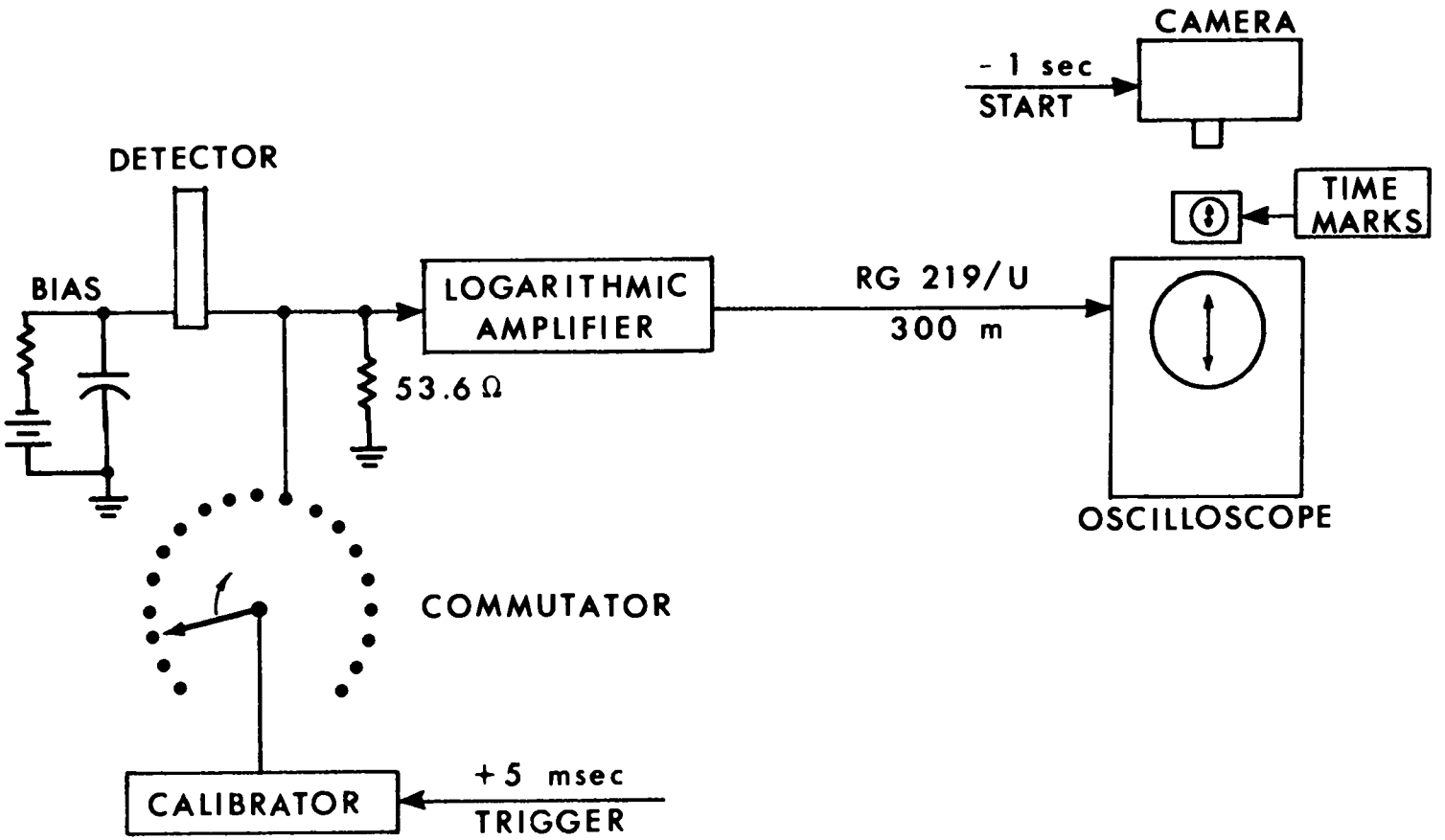

Fig. 3. Simplified schematic of the electronics and associated equipment used for signal recording.

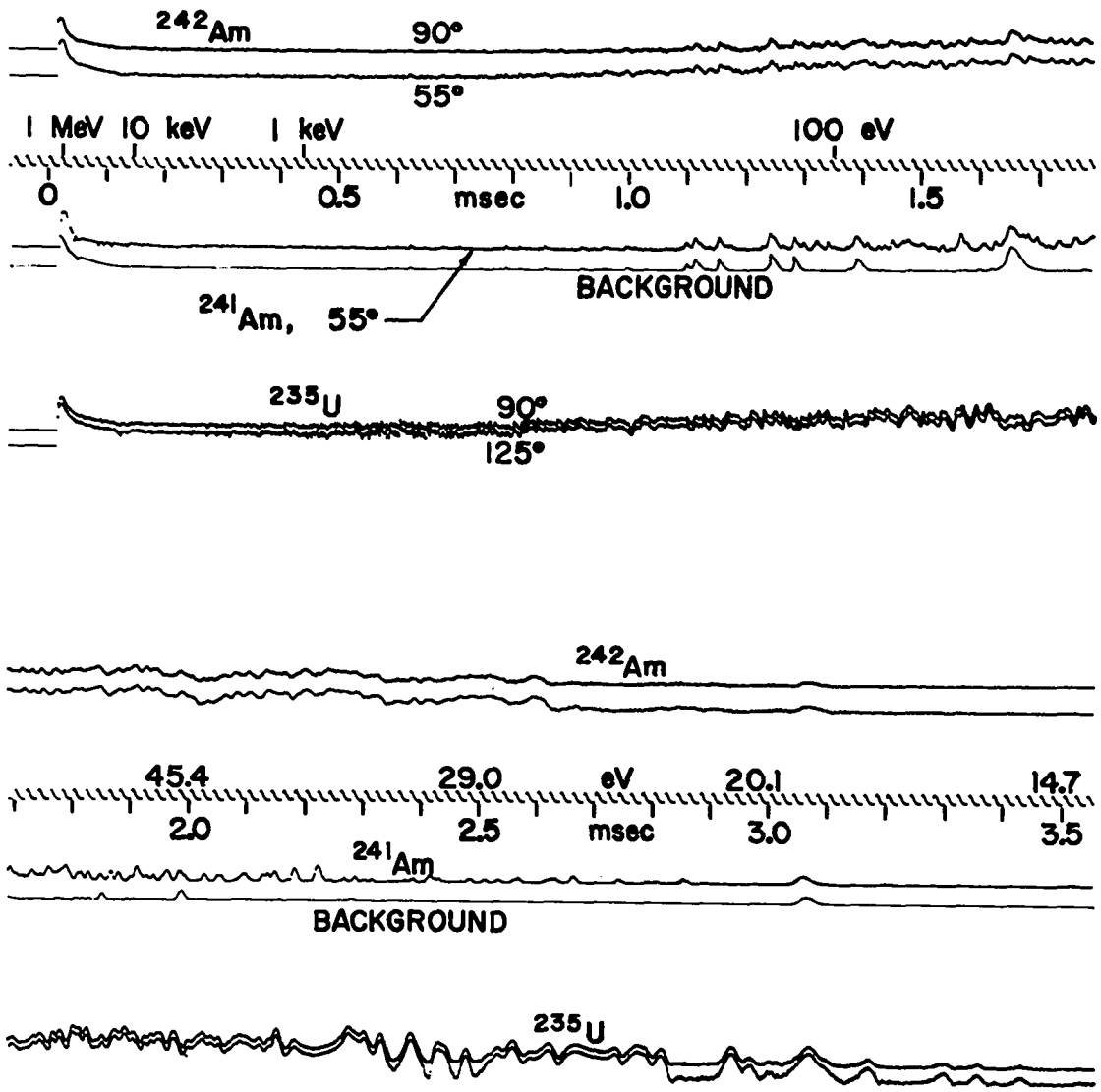

Fig. 4. Typical streak film showing a 10 cm section of six signal traces and the reference trace.

signals on three dual beam oscilloscopes are displayed; the film speed was about 30 μm/μsec. The length of film shown is approximately 10 cm; a one decade change in the signal level at the amplifier input appears as a 600 μm displacement on the film, or about 1.7 mm on Fig. 4. Each such film contains, in addition to the data traces, a reference trace (third from the top) providing both baseline and timing information. The timing pulses were provided by a crystal-controlled 20-μsec pulse generator.

Figure 5 shows the 8-step calibration signal for four of the signals shown in Fig. 4; the calibration steps covered the expected range of the amplifiers. A commutator (diagrammed in Fig. 3) was used to calibrate the amplifiers in sequence at the rate of one amplifier every millisecond beginning 5 msec after the explosion. (At this late time the neutron signal had disappeared.)

Figure 6 displays a portion (2.5 cm) of a typical film recorded in the raster mode, in which the time-base is provided by sweeping the oscilloscope beam in the time direction by means of a free-running crystal-controlled 20 μsec sawtooth generator, while the film is moved past the oscilloscope face perpendicular to this motion. The continuous motion of the film separates and slants the traces. The data signal deflected the trace in opposition to film motion. The trace velocity for this film was about 300 μm/μsec. This example displays four data signals from two dual beam oscilloscopes. The baseline reference trace shown at the top was derived from the same sawtooth generator used for timing the streak records and the raster generator.

The upper part of Fig. 7 displays an example of the 8-step raster calibration superimposed on 1 μsec square-wave time marks; a single beam 'scope is shown for simplicity.

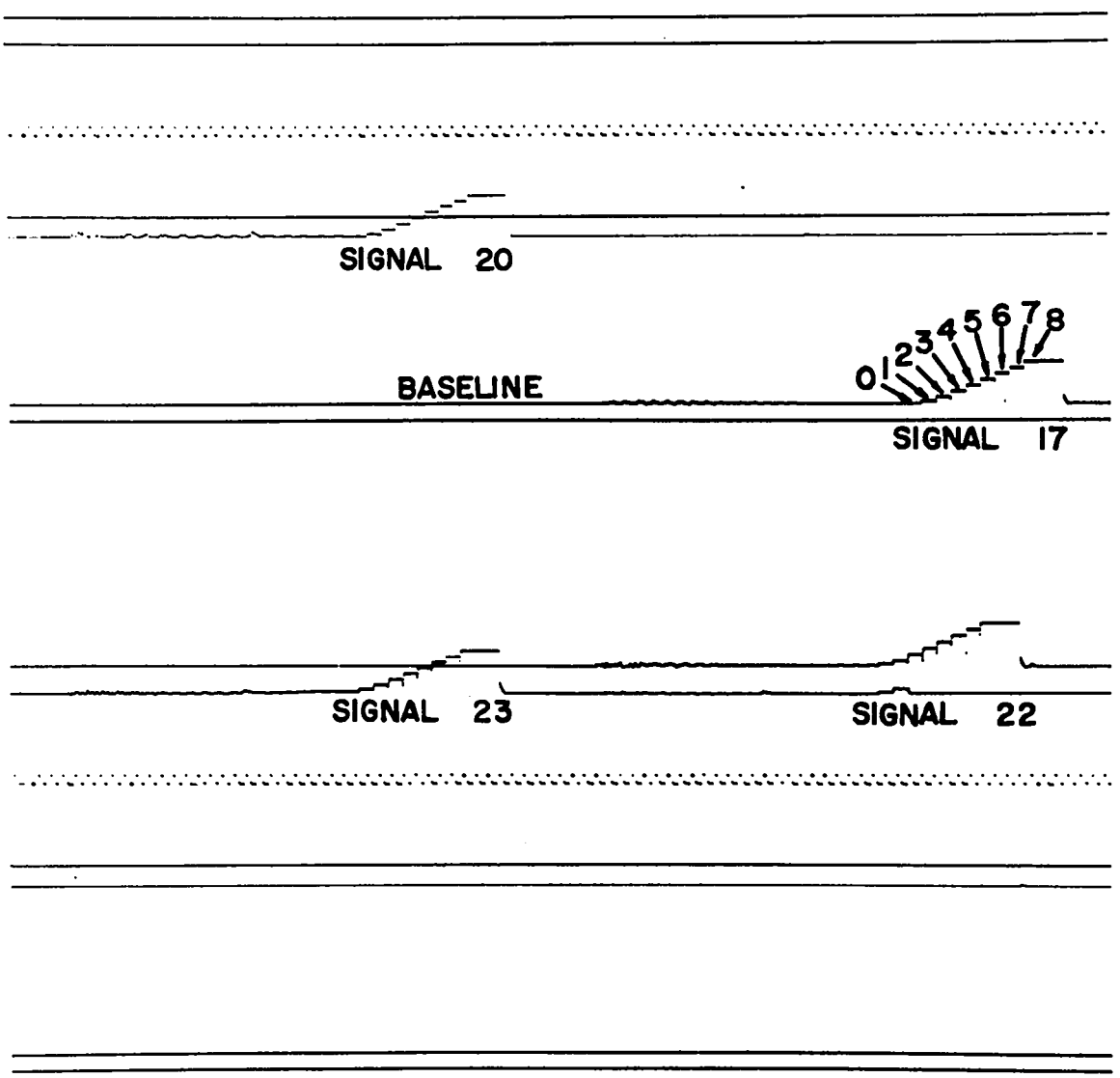

Fig. 5. Typical streak calibration.

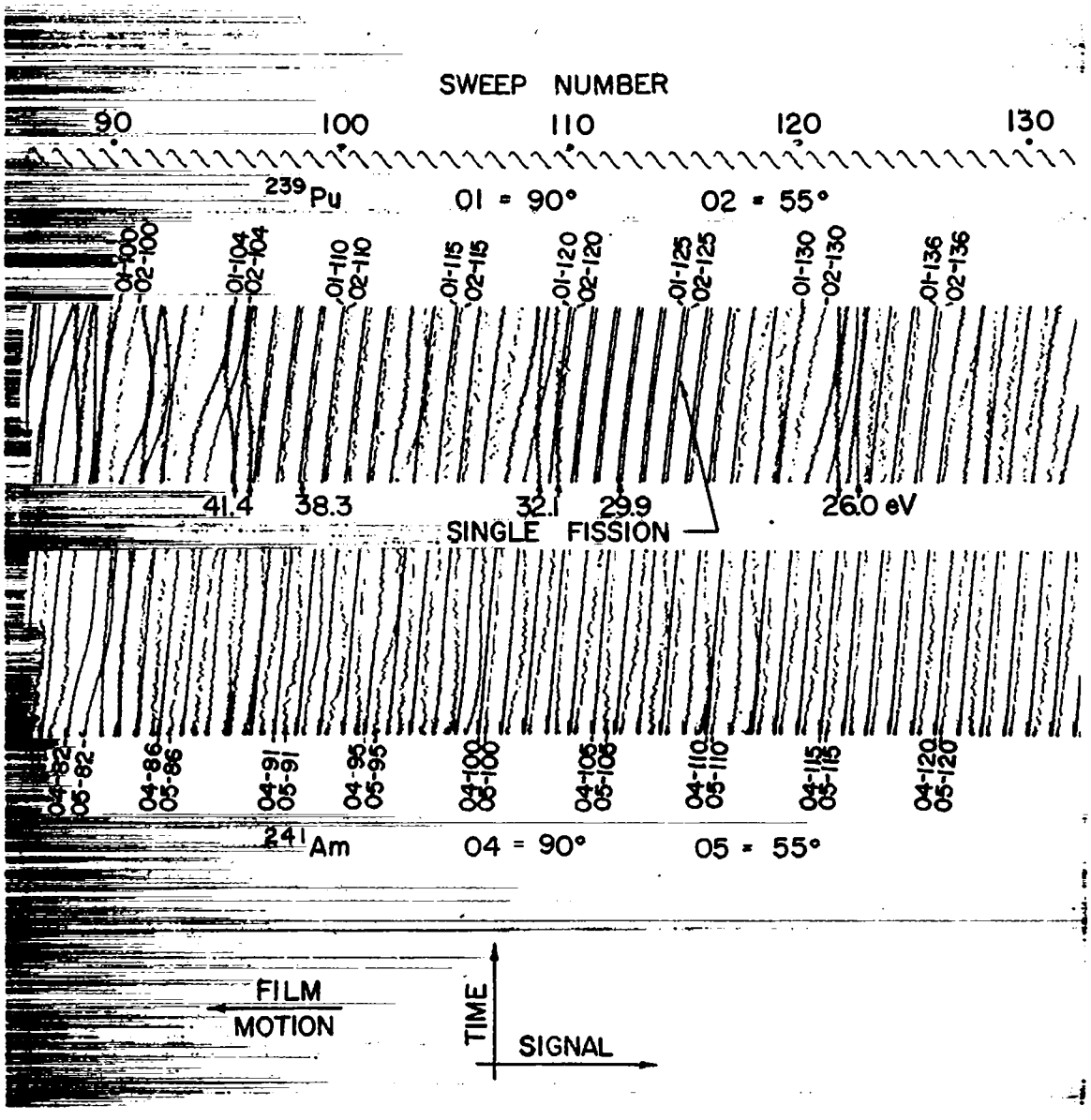

Fig. 6. Typical raster data film showing traces from two dual beam 'scopes.

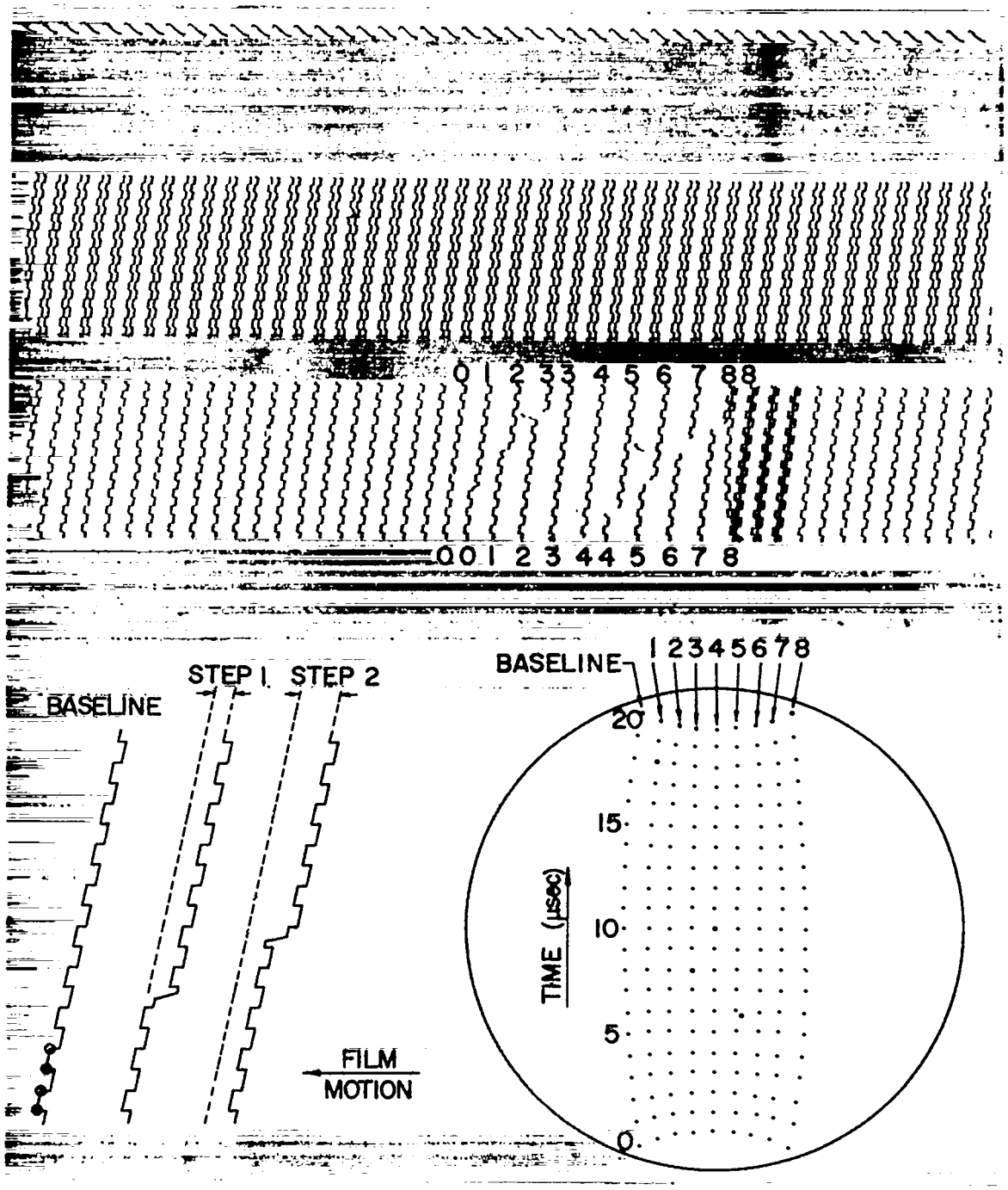

Fig. 7. Raster calibration film and diagram.

The lower right hand part of this figure illustrates how readings of the curves (circled points) provided a 2-dimensional map of the 'scope face and automatically took into account distortions in the oscilloscope and camera. A signal reading from the film, in general, would fall inside of some four point rectangle of calibration points permitting both a time and signal height interpolation to be made.

C. Data Reduction

All films were read at Los Alamos on a Richardson rear projection microscope with Datex digitizers and magnetic tape drive. Independent readings were provided by New Mexico State University using a Telereadex 29-E front projection system. The digitizer unit size was about 1.5 μm for each machine. Thus, since the signal displacement was about 600 μm/decade and each data point was based on reading both the reference and signal trace, the inherent error in reading was about 1%. Reproducibility of readings and distortions in the reader and line width on the film increased this error to about 5% in the worst cases. Timing errors were about 0.1 μsec for streak and 0.015 μsec for raster.

In digitizing a selected film, points were read at close enough intervals to realize the resolution inherent in the record. For convenience the complete digital record from a given trace containing presignal baseline (a good zero signal level reference), signal, baseline reference signal points, and calibration information were stored on magnetic tape.

The information on the tape was converted to signal, S(t), in millivolts as a function of time by comparing the

ordinate of each datum point to the calibration ordinates, applying the known calibration signal levels and interpolating. For streak records, the time scale (X coordinate) was derived from the readings of the baseline reference trace pulse positions (20 μsec separation) which were interspersed on the input data tapes with the signal readings. The zero of the time scale was set arbitrarily to the timing pulse read prior to the onset of data. The time assigned to each signal reading was determined by a linear extrapolation from the X coordinates of the last two baseline-reference pulse positions read. Raster signals are considerably more complicated but the conversion was handled in a comparable manner. A graph of S(t) obtained from a portion of the ^{235}U signal shown as the lowest trace in Fig. 4 is shown in Fig. 8.

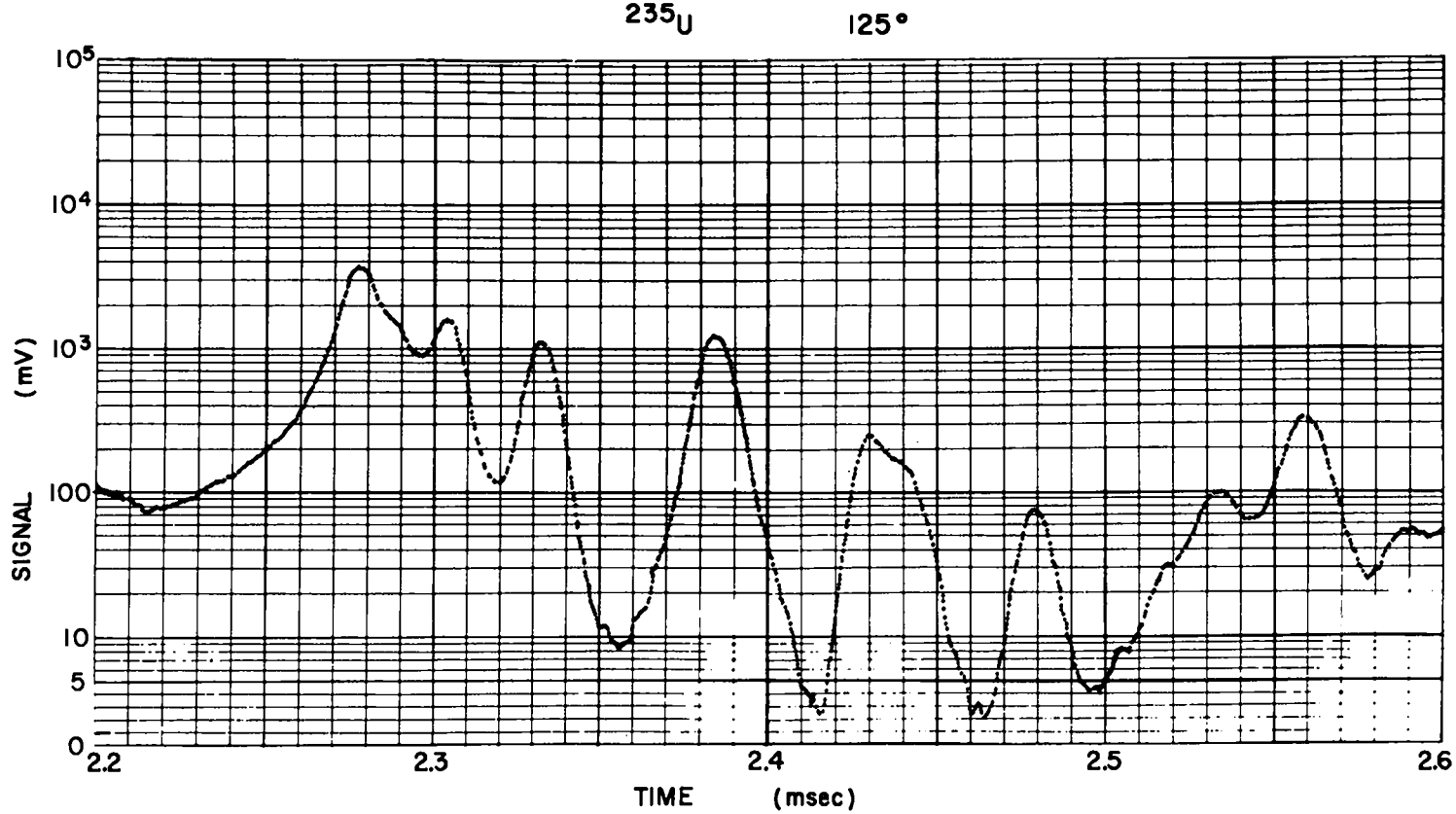

Fig. 8. A section of the signal as a function of time--derived from the 125° ^{235}U signal shown in Fig. 4.

II. ^{233}U FISSION AND CAPTURE CROSS SECTION

A. General Procedure

In the Petrel experiment in which the detector-foil geometries were essentially identical for a number of foils and in which the number of neutrons passing through all foils was approximately the same, the relative cross section of the nuclide of one target to that of another is obtained quite trivially from a simple ratio. Thus, if the cross section of the isotope contained on any one foil is known, all cross sections may be established relative to it. This procedure in a slightly more complicated form was used to determine the cross sections for ^{233}U.

The usual reaction rate expression was used,

$$R = \sigma N f, \tag{1}$$

where R is the reaction rate, σ the cross section, N the areal density of target atoms, and f the incident flux. The observed signal is related to the reaction rate,

$$S(t) = R \cdot \frac{\Omega}{4\pi} \cdot e \cdot \bar{E} \cdot C + B(E), \tag{2}$$

where Ω is the solid angle subtended by the detector and e the efficiency of the detector, $\bar{E}$ is the average energy of the detected particles, C is a conversion factor from energy loss in the detector to mV signal level, and B(E) is the background signal level at the energy E corresponding to time t. It is important to note that since the final results

involve ratios of two signals, the conversion factor C need not be known precisely and only relative values of N, Ω, e, and $\bar{E}$ are required. The value used for C is 0.00242 mV-μsec-MeV^{-1}, based on 3.55 eV per ion pair in Si, electron charge = 1.6 x 10^{-13} μC, and a 53.6 Ω resistor at the amplifier input.

The time coordinates on the S(t) data tapes were based on an arbitrary zero time. Transformation to an energy scale requires knowledge of the flight path and zero time. The flight path D was established prior to the experiment (on Petrel the flight path was set to the distance from the foil to the surface of the moderator located 40 cm above the nuclear device; 184.98 m for the fission foil). This provided an accurate flight path for moderated neutrons but introduced a very small error for the fast neutrons of the fission peak. The zero time, t_o, was adjusted to the arrival time of γ-rays (mid-point on the leading edge of the γ-flash peak) corrected for their flight time of 0.63 μsec. The relation used for energy conversion was

$$E = 5226.68 \left(\frac{D}{t-t_o}\right)^2 \quad eV$$

where D and t have the units of meters and microseconds, respectively. In the calculations the S(t) data were averaged in channels of fixed time width as this conversion was made. The time channel was 0.1 μsec for raster films and 1.0 μsec for streak films, but was lengthened by the program at low energies to approximately 1/8 the Doppler width, (full width at 1/e)

$$\Delta t = 2\frac{\sqrt{mkT}}{\sqrt{ME}}\, t,$$

where m = neutron mass
M = target mass
T = absolute temperature
k = Boltzmann constant
E = energy
t = time.

B. Background Determination

The fission foils were all backed by 13 μm of Pt; the background signal was obtained from a Pt foil identical to this backing, in the same manner as the other signals. This signal was subtracted from all charged particle signals before cross section computations were carried out. The background, shown in Fig. 9, was quite low except at the highest energies and at the isolated Pt resonances (compare Figs. 8 and 9). The derivation of the background B(E) was performed using eq. 2 with the information from the background detector (signal 20 of Fig. 4) used for S(t), omitting the B(E) term and setting all other coefficients to unity.

C. Flux Determination

The flux was established by subtracting the background from the flux signals (^{6}Li and ^{235}U), setting the "flux" in eq. 2 to the known cross sections listed in Table 1, and plugging in the appropriate numbers for N, e, and $\bar{E}$. In the final result the flux shown in Fig. 10 was determined by ^{235}U σ_f above 10 keV and the ^{6}Li(n,αt) reaction for lower energies.

The high energy spectrum was that of fission neutrons. A slowing-down spectrum extended from this energy to about 320 eV and at lower energies the "thermal" neutrons dominated

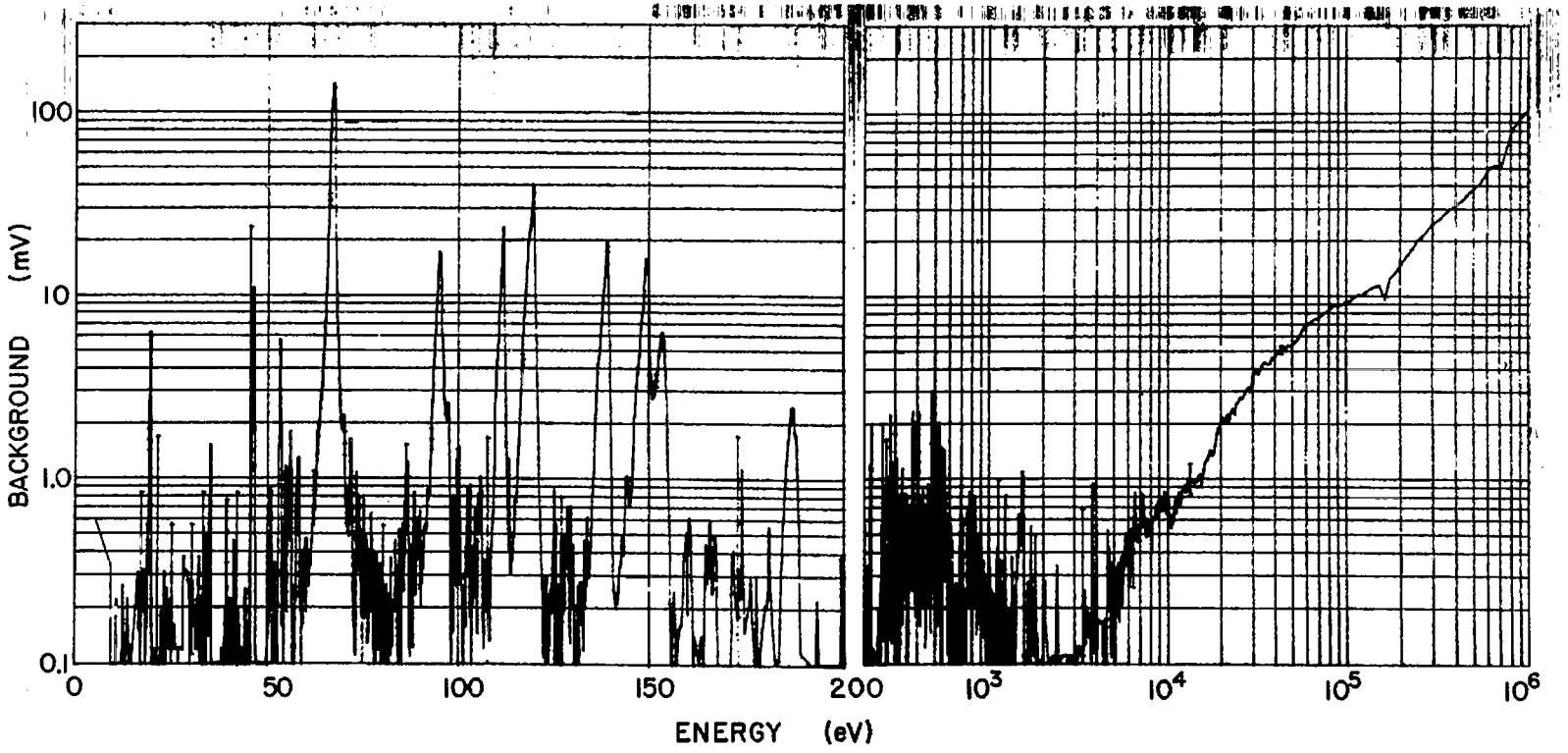

Fig. 9. Background signal.

TABLE 1(a)

Fission Cross Section of ^{235}U Used for Normalization[12]

E(eV)	σ(barns)	E(eV)	σ(barns)	E(eV)	σ(barns)
1.0×10^6	1.23	1.6×10^5	1.47	4.0×10^4	2.09
9.5×10^5	1.20	1.5	1.49	3.8	2.12
9.0	1.18	1.4	1.52	3.6	2.15
8.0	1.18	1.3	1.54	3.4	2.18
7.0	1.19	1.2	1.57	3.2	2.22
6.0	1.20	1.1	1.60	3.0	2.27
5.5	1.21	1.0×10^5	1.63	2.8	2.31
5.0	1.22	9.0×10^4	1.68	2.6	2.36
4.5	1.23	8.0	1.73	2.4	2.41
4.0	1.25	7.5	1.75	2.2	2.47
3.5	1.28	7.0	1.78	2.0	2.55
3.0	1.32	6.5	1.82	1.8	2.64
2.8	1.33	6.0	1.86	1.6	2.72
2.6	1.34	5.5	1.90	1.4	2.83
2.4	1.36	5.0	1.95	1.2	2.95
2.2	1.38	4.7	1.99	1.0×10^4	3.23
2.0	1.41	4.4	2.03		
1.8×10^5	1.44	4.2×10^4	2.05		

TABLE 1(b)

$^6Li(n,\alpha)t$ Cross Section Used for Normalization[13]

E(eV)	σ(barns)	δσ/σ	E(eV)	σ(barns)	δσ/σ
1.0×10^4	1.518	0.04	4.0×10^3	2.377	0.036
9.0×10^3	1.598	0.04	3.0	2.740	0.034
8.0	1.692	0.04	2.0	3.351	0.032
7.0	1.806	0.04	1.0×10^3	4.732	0.03
6.0	1.947	0.04	1.0×10^2	14.964	0.03
5.0×10^3	2.129	0.038	1.0×10^1	47.32	0.03

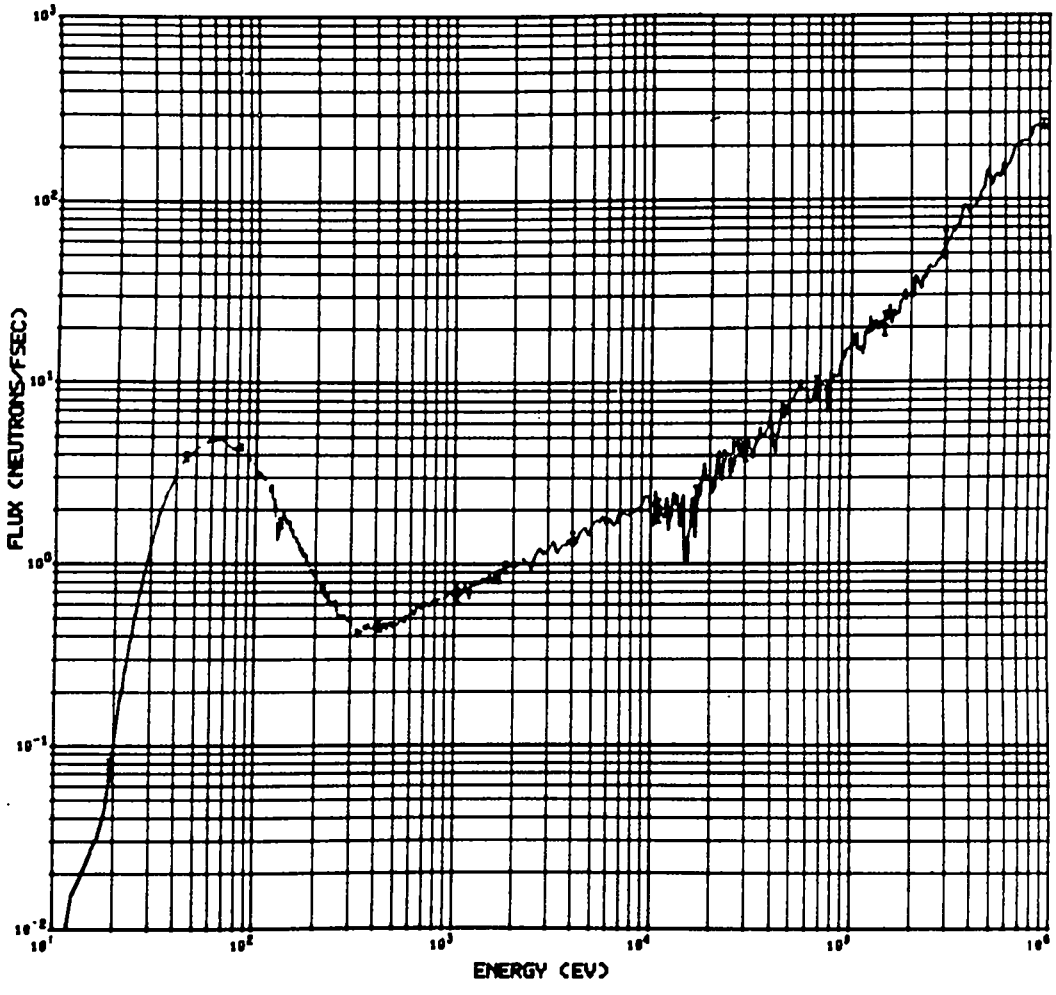

Fig. 10. The neutron flux (neutrons per 10^{-15} sec as a function of energy) determined by the $^{6}Li(n,\alpha t)$ up to 10 keV and $^{235}U(n,f)$ at higher energies.

the flux. The apparently high temperature of the "thermal" peak was caused by neutron, gamma, and shock compression heating superimposed on moderator motion. Neutrons which were thermalized by the moderator were delayed until shock compression and heating "boiled" them out; concurrently, the pressure wave accelerated the moderator up the pipe and the high thermal temperature and moderator velocity produced the "Maxwellian" flux peak at 60 eV. The rapid cutoff at about 20 eV was due to the sweeping up of low energy neutrons by the moving moderator. The actual displacement of the moderator during neutron emission, however, was negligible.

The time delay due to diffusion of neutrons in the moderator was three μsec as determined by the location of well known peaks in ^{240}Pu and Pt both above and below 320 eV.[14] This delay was taken into account in computing the cross sections.

Nickel neutron windows were used on the vacuum pipe and the Ni apparently contained a trace of Co; the two elements have neutron resonances which produced the flux dips at 130 eV (Co) and 15 keV (Ni).

D. Fission Cross Section Determination

The fission cross sections were determined from eq. 2 using the background and flux described in Secs. B and C. The remaining coefficients were determined by the various means discussed below.

E. Capture Cross Section

The capture + fission cross section was derived from the γ-ray (Moxon-Rae type) detector. The conversion of signal to cross section was carried out in the same

manner as that for the fission signal with the background subtraction omitted. (The signal recorded from the low reaction cross section Bi_2O_3 target was negligible below 1 keV.) Because of inadequate information on the detector efficiencies for the fission and capture γ-rays, the final cross sections were normalized to the fission data. In the region of a broad fission resonance (the one at 34 eV was used) the capture-to-fission ratio, α, will be quite small; the assumption $\alpha = 0.1$ is close enough to reality to produce a reasonably accurate value of $\sigma_c + \sigma_f$, the capture + fission cross section; the sum $\sigma_c + \sigma_f = (1 + \alpha)\sigma_f$ is then normalized to the fission data. The detector efficiency as computed from the normalization (see Table 2) was compared to that determined from the ^{240}Pu capture signal. For ^{240}Pu the efficiency was determined at a "black" resonance where the reaction rate was determined by the flux. The treatment of the two nuclides differs in that fission γ-rays create most of the ^{233}U signal at the normalization energy, and capture γ-rays produce the ^{240}Pu signal. While the γ-ray detector was designed to have an output proportional to the incident flux of gamma ray energy, the two results differ by 30%. (This is not a surprising result since the γ-ray energy produced by fission is greater than the Q value of the capture reaction by a similar percentage.) As a result of this difference the systematic error for the ^{233}U was set high.

Because the capture target was thick, the computed cross section was also corrected for flux degradation according to the equation

$$\sigma = \frac{1}{N} \ell n \left(\frac{1}{1 - N\sigma_e} \right)$$

where N is the target thickness in atoms/barn, and σ_e is the uncorrected cross section.

F. Parameter Determination

The fission and ^{6}Li foils (in the form of UO_2 and LiF) were made by J. Povelites of this Laboratory using the vacuum evaporation technique. The diameter of the deposit was 5 cm, a size designed to assure containment of the 1.9 cm diameter neutron beam. The mass of the ^{6}Li foil was established by weighing. The amount of fissile material on the ^{233}U and ^{235}U foils was determined by measuring their thermal fission rate, and combining the results of alpha counting and chemical assay (of ^{235}U only) with the isotopic abundances determined by mass spectrometry. With the knowledge of the foil areas as determined by the evaporation geometry, the areal density was found by combining the results of all mass measurements (in the form of number of atoms) and the foil area; an additional factor of $\sqrt{2}$ enters because the foils were at 45^o to the beam. The capture foil was a 0.20 mm thick, 4.1 cm diameter disk of ^{233}U metal (isotopic composition approximately the same as the fission foil) encapsulated in 0.25 mm thick aluminum. Its mass was determined by weighing, and size by radiography. Table 2 shows the ^{233}U foil composition (a) and estimated thickness and correlated error (b).

The differences in efficiency e between charged particle detectors were determined by measuring the counting rate for each detector when exposed to a radioactive source under conditions of identical geometry. All signals were normalized to the ^{6}Li flux detector. In addition to the actual counter efficiency, the factor e includes the effect of the beam being off the center line of the target array

TABLE 2(a)

Composition of ^{233}U Foils

Isotope	Fission Foil	Capture Foil
^{233}U	97.96 ± 0.05%	97.79 ± 0.05%
^{234}U	1.37 ± 0.04	1.49 ± 0.05
^{235}U	0.07 ± 0.03	0.09 ± 0.03
^{238}U	0.6 ± 0.04	0.63 ± 0.05

TABLE 2(b)

Foil-Detector Information

Foil	Atom Density, N (atoms/barn)	Relative Error δN/N	Detector Efficiency
^{6}Li	1.67×10^{-5}	0.05	1
^{235}U	1.864×10^{-6}	0.02	1.030
^{233}U fission	1.632×10^{-6}	0.03	1.022
^{233}U Capture	1.63×10^{-3}	0.05	0.054

Foil	Q (MeV)	$\bar{E}$ (MeV)	Systematic Error referred to ^{6}Li	Systematic Error referred to ^{235}U
^{6}Li	4.787		0	-
^{235}U	171.5	48.2	-	0
^{233}U fission	173.1	42.4	0.079	0.060
^{233}U Capture	173.1 n,f* 6.77 n,γ	.15	.15	.15

*Only about 8 MeV of the reaction energy appears as γ-rays.

due either to a shift or tilt of the experimental station. The beam was determined to have been 0.25 cm off center at the top of the station by autoradiographs of special targets, presumably due to tilt. The corresponding maximum solid angle change would then be 4%; the estimated error was increased by 1% per target position away from the standard. Another factor entering into e is that of time dilation resulting from using flux per unit time which for a given energy varies with source distance. The efficiency factor e, therefore, includes the ratio of the distance to the ^{6}Li target to the distance to the target in question as a multiplying factor. The resulting values for e are shown in Table 2(b).

The average fragment energy, $\bar{E}$, deposited in the detector depends on the Q-value and the foil and detector dead layer thicknesses. $\bar{E}$ was determined for dead layer thicknesses used in the experiment by bombarding the ^{235}U Petrel foil with thermal neutrons, recording the fragment energy distribution and deriving the average energy. The Q-values for the fissile targets, also important to the center-of-mass correction, were calculated according to the mass law equation $Q = 0.22Z^2/A^{1/3} - 3.4A^{2/3}$ and are shown in Table 2. The correlated error in Table 2(b) includes all errors which affect each data point in a similar manner.

G. Results and Comparison to Other Data

The measured fission cross section is shown in Fig. 11, and $\sigma_f \cdot \sqrt{\bar{E}}$ is plotted in Figs. 12 and 13. A complete listing of the data may be found in Ref. 8 (in which data have been revised above 10 keV from that shown in Ref. 2). Comparisons have been made between these data and those of previous measurements;[15-20] the results are

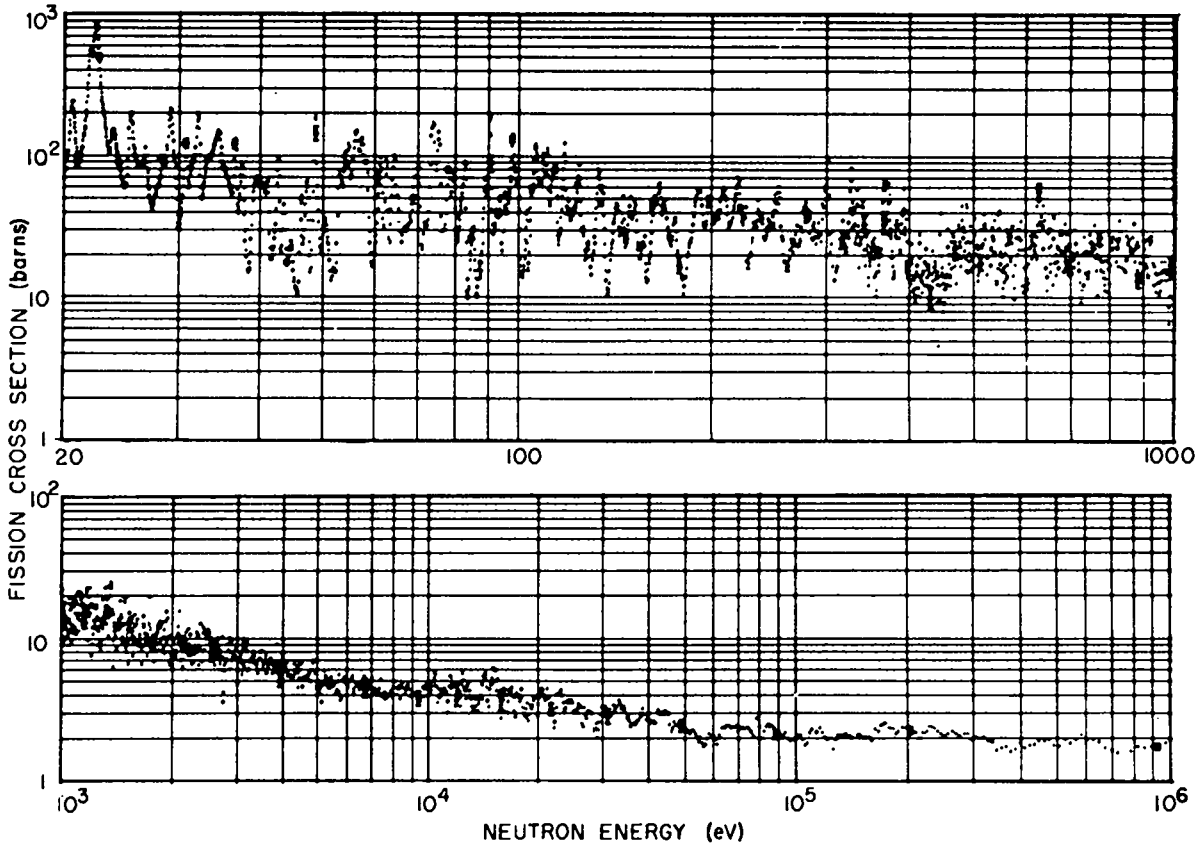

Fig. 11. ^{233}U (n,f) cross section from 20 eV to 10^6 eV.

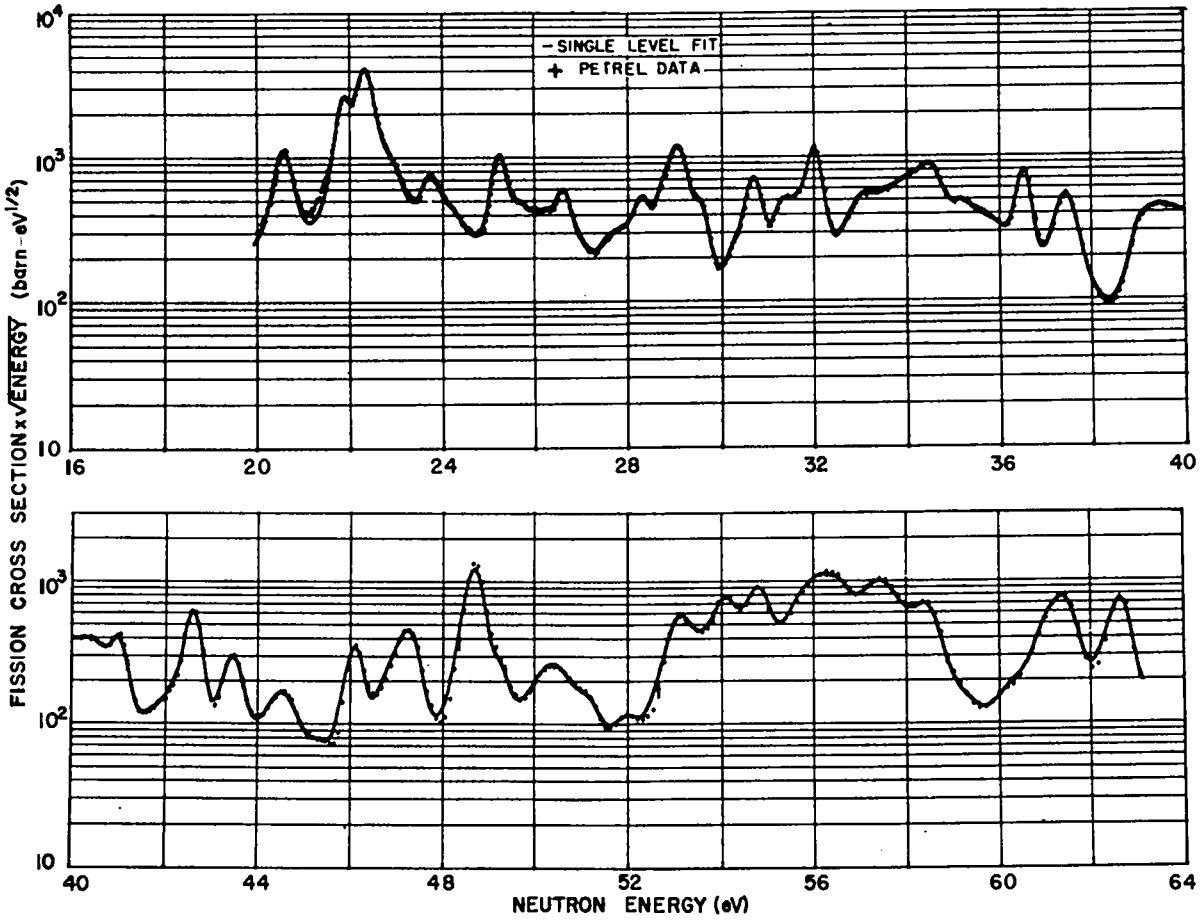

Fig. 12. Single level fit to the fission data.

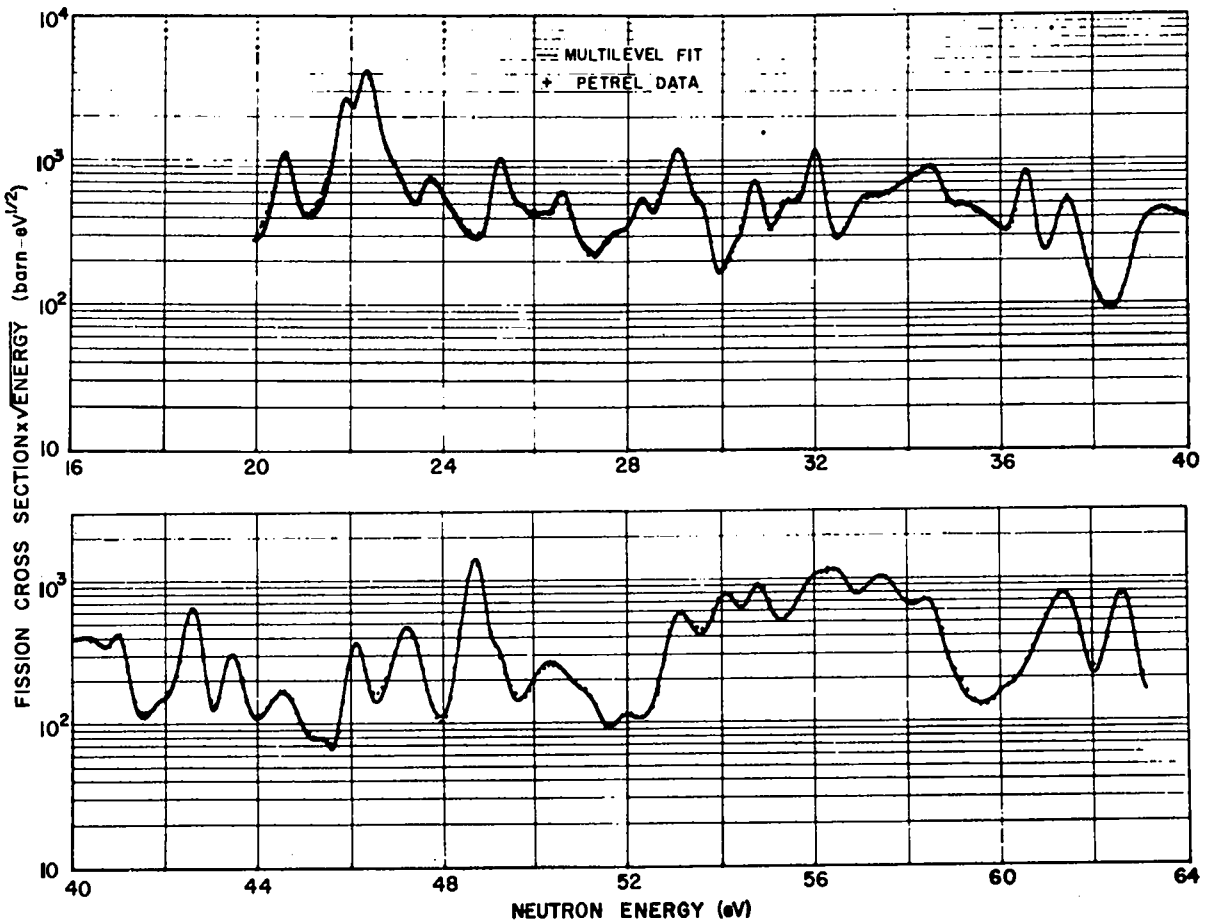

Fig. 13. Multilevel fit to the fission data.

included in Table 3. The general structure of the low energy data agree with those of Refs. 15 and 16; however, the low energy cross section values do not agree. A discrepancy also exists in the energy scale between Nifenecker's results[16] and the Petrel measurements. The validity of the energy scale presented here is verified by the good agreement of the Petrel data on ^{235}U, ^{239}Pu, ^{240}Pu, and Pt with previous measurements.[21]

The data of Refs. 15 and 16 are some 30-50% lower than the Petrel data; in fact, from 20 to 2000 eV the Petrel data exceed the total cross-section measurements of Pattenden and Harvey.[17] The Petrel data were obtained from the 125° detector (see Fig. 2). The results of a second detector placed at 90° and the capture + fission signal from the Moxon-Rae type γ-ray detector have been compared to the 125° signal and give consistent results. The γ-ray signal, of course, differs from resonance to resonance compared to the fission signal, but when averaged over several eV the ratio of the two signals agrees well from 24 to 2000 eV. This may be fortuitous because at the energy of each resonance in ^{240}Pu and Pt the flux was altered between the fission and γ-ray foils.

At the higher energies the agreement between the various sets of data appears fairly good; the Petrel data is some 20% above the 24 keV measurement of Perkin et al[20] but fall slightly below those listed in Ref. 21 above 10^4 eV.

A portion of the ^{233}U capture + fission cross section is shown in Fig. 14 (cross section x $\sqrt{E}$). Only this region is presented because the resonances in the intervening ^{240}Pu capture foil and the Pt foil backings distorted the flux and rendered an accurate interpretation of the data nearly impossible (note that data are omitted at 38 and 41 eV due

TABLE 3

Comparison of Average Cross Section for Selected Intervals

E_1 (eV)	E_2 (eV)	$\bar{\sigma}_f$ Petrel (barns)	Moore[15] (barns)	Nifenecker[9] (barns)	Albert*[18] (barns)	James[19] (barns)	Perkin[20] (barns)
20.0	27.3	182.0 ± 14.	83	104.1			
27.3	38.4	87.1 ± 7.0	43	59.3			
38.4	51.6	41.1 ± 3.3	23	30.0	46		
51.6	66.0	67.5 ± 5.4	34		50		
66.0	83.7	58.4 ± 4.6	29		35		
83.7	102.	48.6 ± 3.8	27		38		
102	130	53.7 ± 4.3	32		30		
130	159	32.8 ± 2.6	20		28		
159	195	34.0 ± 2.7	14		27		
195	260	37.8 ± 3.0	19		28.5		
260	320	30.6 ± 2.4	17		32.8		
320	500	23.9 ± 1.9	14		21		
500	1.0×10^3	20.4 ± 1.6	12		12.7		
1.0×10^3	2.0	12.4 ± 1.0			9.97	9.39 ± 0.9	
2.0	3.0	8.62 ± 0.69			7.93	7.61 ± 0.8	
3.0	4.0	6.83 ± 0.55			6.16	5.95 ± 0.6	
4.0	6.0	5.25 ± 0.42			6.07		
6.0	8.0	4.49 ± 0.36			5.24	4.80 ± 0.4	
8.0	1.0×10^4	4.24 ± 0.34			4.90	4.26 ± 0.4	
1.0×10^4	1.5	4.28 ± 0.34			4.03	3.49 ± 0.3	
1.5	2.0	3.78 ± 0.3					
2.0	3.0	3.26 ± 0.26					2.73 ± 0.11 (24 keV)
3.0	5.0	2.81 ± 0.22					
5.0	1.0×10^5	2.23 ± 0.18					
1.0×10^5	2.0	2.18 ± 0.18					
2.0	4.0	2.00 ± 0.16					

*Interpolated from reported values.

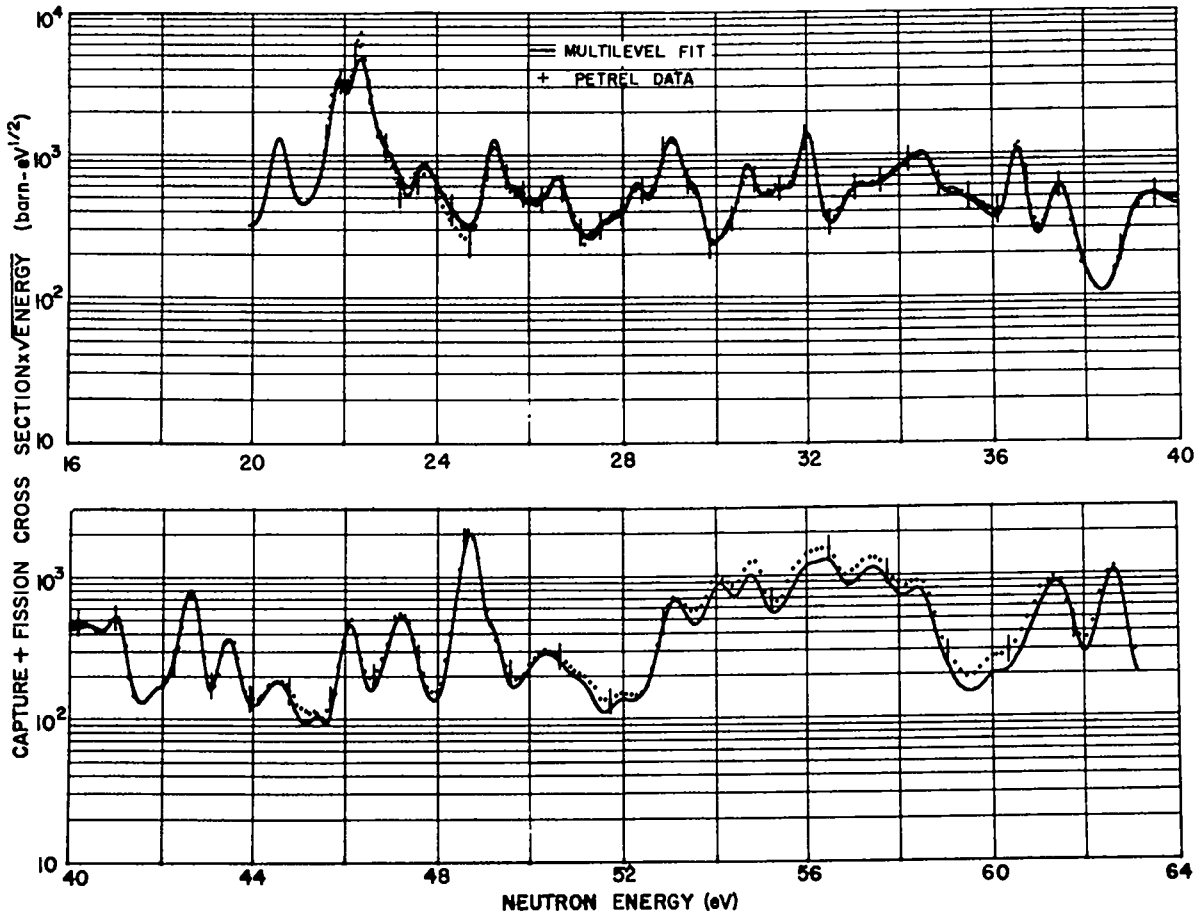

Fig. 14. Multilevel fit compared to the Petrel ^{233}U (n,f) + ^{233}U (n,α) data.

to ^{240}Pu resonances). The data of the ratio α are presented in Fig. 15 and again in Fig. 16 (data below 28 eV were omitted because of the increased statistical error resulting from the weaker flux--see Fig. 10). A scaling error may exist for these data since the relative efficiency of the γ-ray detector for fission and capture γ-rays is poorly known and was assumed to be the same for each reaction (see p. 23).

Because of the thick target correction made to the γ-ray data, significant errors in the cross section data should manifest themselves at regions of high cross section. At the 22 eV resonance the peak appears to have been over-corrected (see Fig. 14) indicating that the fission cross section used for normalization was too large. The reduction in the fission cross section required to remove this distortion ranges between 15 and 30% and does not appear to account entirely for the 30-50% error between these data and those of Refs. 15 and 16.

H. Treatment of Errors

The systematic error listed in Table 1 includes those errors which affect all data equally. The sources of this error are the error in isotopic composition, areal density, Q value, average deposited energy ($\bar{E}$), geometry, and efficiency.

Sources of error which vary with energy or signal level are included with the statistical error. These include the rms deviations of the calibration step due to reading error and calibrator jitter, statistical errors of the points, and errors in the background subtraction and flux determination.

The statistical error of a data point is determined by converting the sum of all input signals, S(t), falling

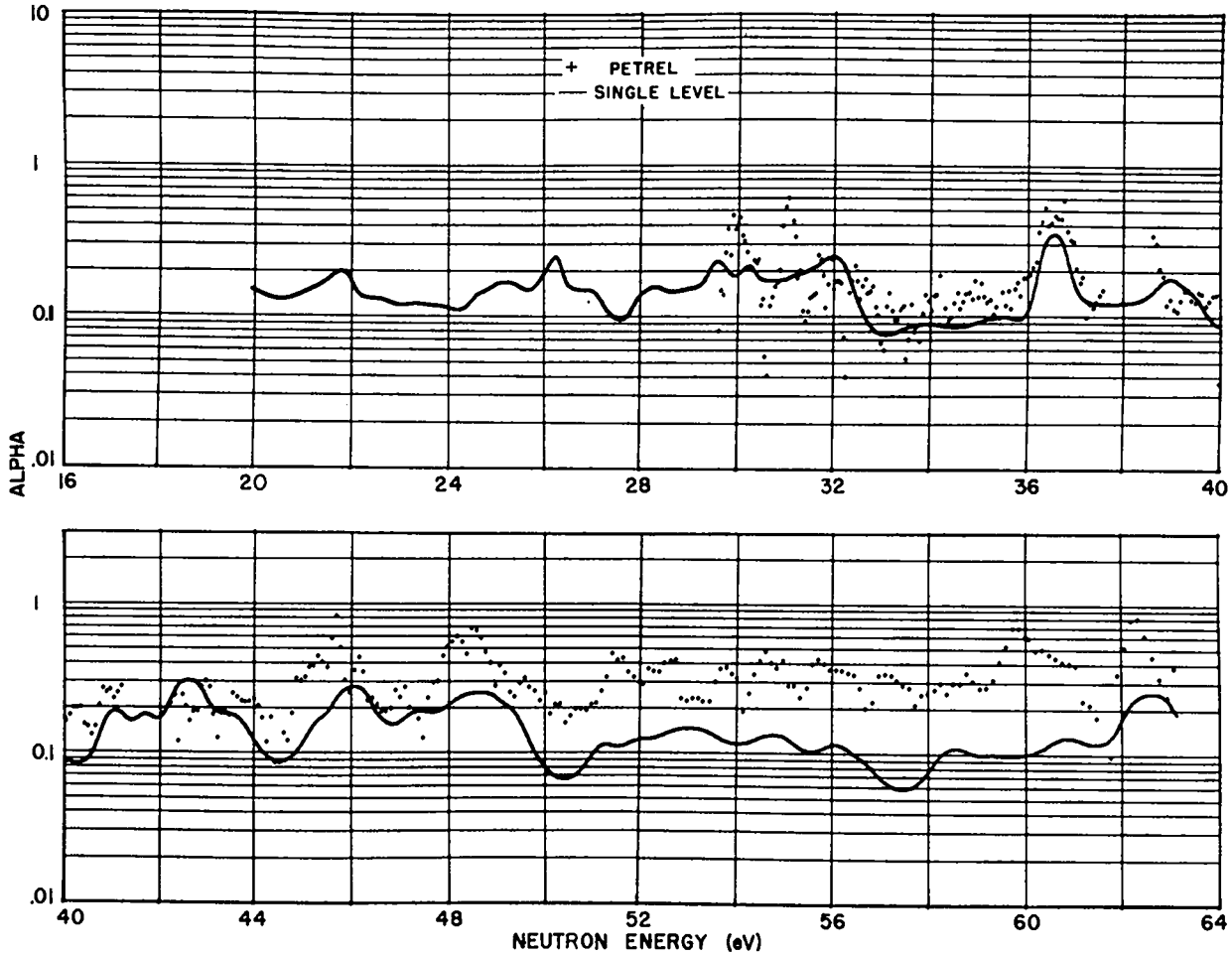

Fig. 15. Single level results compared to the ratio α derived from Petrel ^{233}U data.

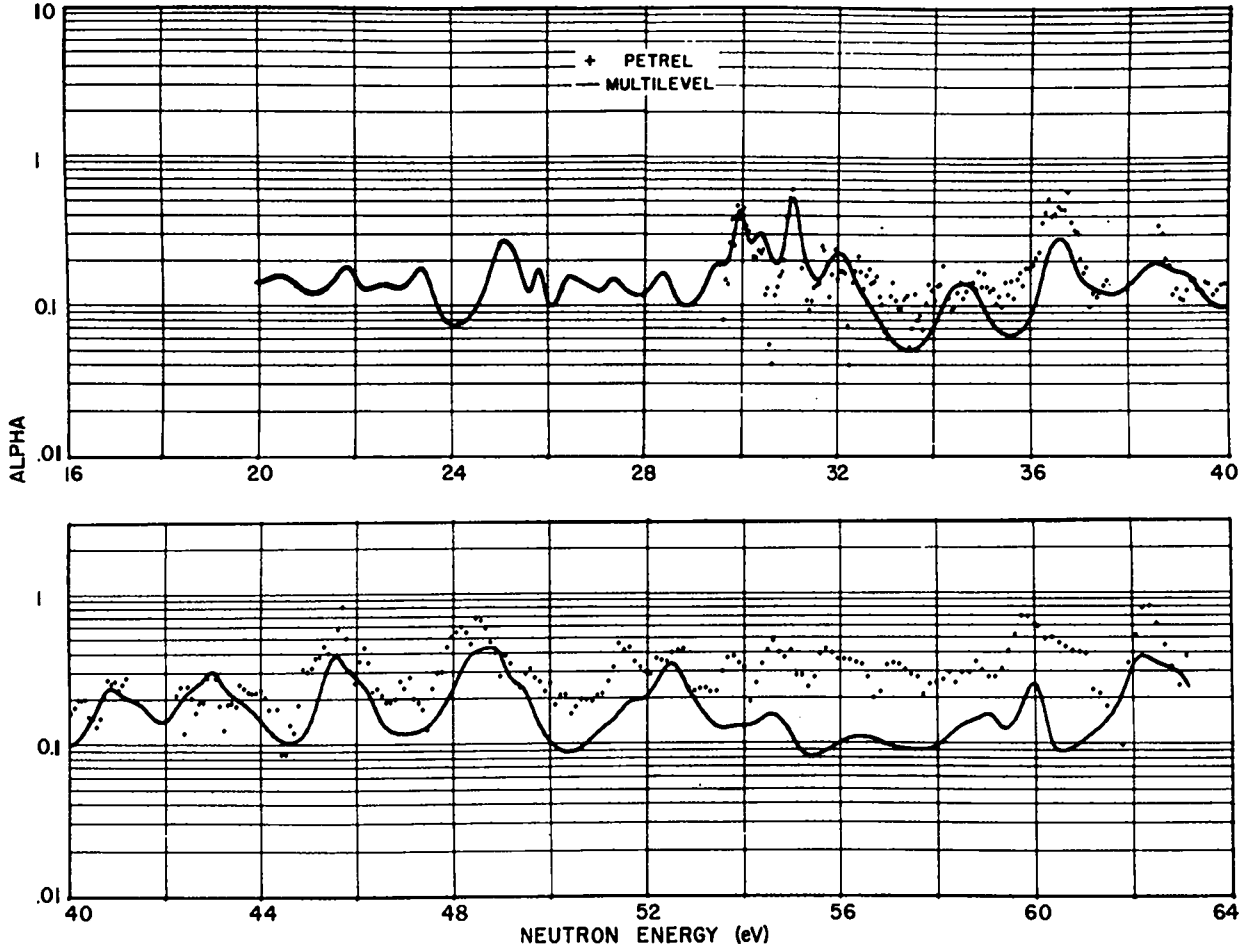

Fig. 16. Multilevel results compared to the ratio α derived from Petrel ^{233}U data.

in the time interval to be represented by the datum point to counts, and comparing the statistical error of this number to the rms deviation of the signal for all points in the time channel; the larger of the two is taken as the statistical error.

The "statistical" errors are shown on the fission data of Figs. 11, 12, and 13. Typical values range from 5 to 10%. The errors shown with the capture + fission data (Fig. 14) include the systematic error and range around 20%. The errors which sould be assigned to the α data are difficult to establish because of the limited information available on the relative response of the γ-ray detector to fission and to capture γ-ray. The statistical errors as defined above range around 10-20% for $(1 + \alpha)$, the ratio of capture + fission cross section to fission cross section.

III. DATA ANALYSIS - LOW ENERGY

A. Method

Theoretical fits have been made previously to the ^{233}U cross sections using both single and multilevel formalisms (0-10 eV multilevel,[22] 0-40 eV single level[9]). The results of the single level approach[9] appear to indicate that interference effects are quite weak for ^{233}U. On the other hand, Lynn[10] argues that the peaks in the observed fission cross sections for a nucleus like ^{233}U are greatly affected by interference and may, in fact, not represent resonances at all.

In order to compare the two methods, and simultaneously gain some insight into the strength of interference between levels, both a single and multilevel fit were made to the Petrel data between 20 and 63 eV. (The experimental resolution did not warrant a fit to higher energies.) It is likely that, because of the many channel nature of the capture reaction, the capture cross section would be very little altered by interference. Peaks in the fission cross section due to a cooperative interference would then show a very low α, while α would be large in deep fission valleys caused by destructive interference. With this in mind the Petrel α data, which are poor but are the best currently available, were used as a measure for the validity of the fit. The fits were therefore performed solely on the fission data, and the resulting resonance parameters were used to compute an α which was compared to the experimental α (Figs. 15 and 16).

The equation used for the single level fit was that of a sum of Breit-Wigner levels[23]

$$\sigma_f(E) = \pi\lambda\!\!\!^{-2} g \sum_\lambda \frac{\Gamma_{n\lambda}\,\Gamma_{f\lambda}}{(E-E_\lambda)^2 + \Gamma_\lambda^2/4}$$

where

$g = (2J+1)/(2s+1)(2I+1)$

J = spin of compound nucleus

I = spin of the nucleus

s = neutron spin

$\lambda\!\!\!^{-}$ = neutron wave length

$\Gamma_{n\lambda}$ = neutron width

$\Gamma_{f\lambda}$ = fission width

$\Gamma_{\alpha\lambda}$ = capture width

Γ_λ = total width $(\Gamma_{n\lambda}+\Gamma_{f\lambda}+\Gamma_{\gamma\lambda})$

and E_λ = energy of resonance λ.

The more complicated multilevel equation is based on the Wigner-Eisenbud formalism[24] as developed for computation purposes by Reich and Moore.[25]

The cross section equation has the familiar form

$$\sigma_{ij} = \pi\lambda\!\!\!^{-2} g \left| \delta_{ij} - S_{ij} \right|^2$$

where ij are reaction channels and the S_{ij} are elements of the Collision Matrix for levels of one spin and parity. S, for s-wave neutrons, may be written as

$$S = \omega \left(\frac{1 + G}{1 - G} \right) \omega \qquad (3)$$

where ω is the diagonalized phase shift matrix and the elements of G for S waves may be approximated as

$$G_{jk} = \frac{i}{2} \sum_{\lambda} \frac{\Gamma_{\lambda j}^{\frac{1}{2}} \Gamma_{\lambda k}^{\frac{1}{2}}}{E_{\lambda}-E}$$

By rewriting eq. (3) in the form

$$S = \omega[2(1-G)^{-1}-1]\omega \qquad (4)$$

S is found by inverting the matrix 1-G. Using the Reich-Moore technique this is done by partitioning G into a 2 x 2 matrix of matrices before inverting.

Thus,

$$G = \begin{pmatrix} G^{\ell x \ell} & G^{\ell x n} \\ G^{n x \ell} & G^{n x n} \end{pmatrix}$$

where index

1 represents the incoming neutron channel

2....ℓ represent the ℓ-1 fission channels

ℓ+1...ℓ+n represent the n capture channels.

Upon performing the inversion required by eq. (4) the fission cross section for a given channel j can be shown to be:[26]

$$\sigma_{1j} = 4\pi\lambda^2 g \left| (1-H^{\ell x \ell})^{-1}_{1j} \right|^2$$

and the capture cross section

$$\sigma_{1\gamma} = \pi\lambda^2 g \sum_{\lambda} \frac{\Gamma_{\gamma\lambda}}{(E_{\lambda}-E)^2 + \frac{\Gamma_{\gamma\lambda}}{4}^2} \left| \sum_{j=1}^{\ell} (1-H^{\ell x \ell})^{-1}_{1j} \Gamma_{\lambda j}^{\frac{1}{2}} \right|^2$$

where

$$H_{lj}^{\ell x \ell} = \frac{i}{2} \sum_{\lambda} \frac{\Gamma_{\lambda l}^{\frac{1}{2}} \Gamma_{\lambda j}^{\frac{1}{2}}}{E_{\lambda} - E - \frac{i}{2}\Gamma_{\gamma\lambda}} .$$

In order to compare the calculated cross sections with the experimental values, account must be taken of the resolution and Doppler broadening. The resolution function was determined by the shapes of the narrow resonances in ^{240}Pu, and is essentially that expected from the moderator (see previous discussion, p.19). The resolution function with which the data were convoluted is shown in Fig. 17.

The Doppler width (half width at 1/e) used for the Gaussian Doppler function was the familiar $\Delta_E = \sqrt{4kTmE/M}$.

The convolution of the computed cross section with the Doppler and resolution functions was performed by numerical integration.

B. Interpretation of Results

According to the fission model proposed by A. Bohr[27] fission can be described as a few channel process. In Bohr's model, a large fraction of the neutron capture excitation energy is converted into potential energy as the nucleus deforms for fission. This reduces the energy available for excitation, and in general only a few simple nuclear modes can be excited. With the addition of a low energy neutron to ^{233}U these modes include only rotation, vibration and combinations of these; i.e., the particle arrangement is much like the ^{234}U ground state.

The nuclide ^{233}U has ground state spin and parity $I^{\pi} = 5/2^{+}$; therefore, the ^{234}U compound nucleus formed

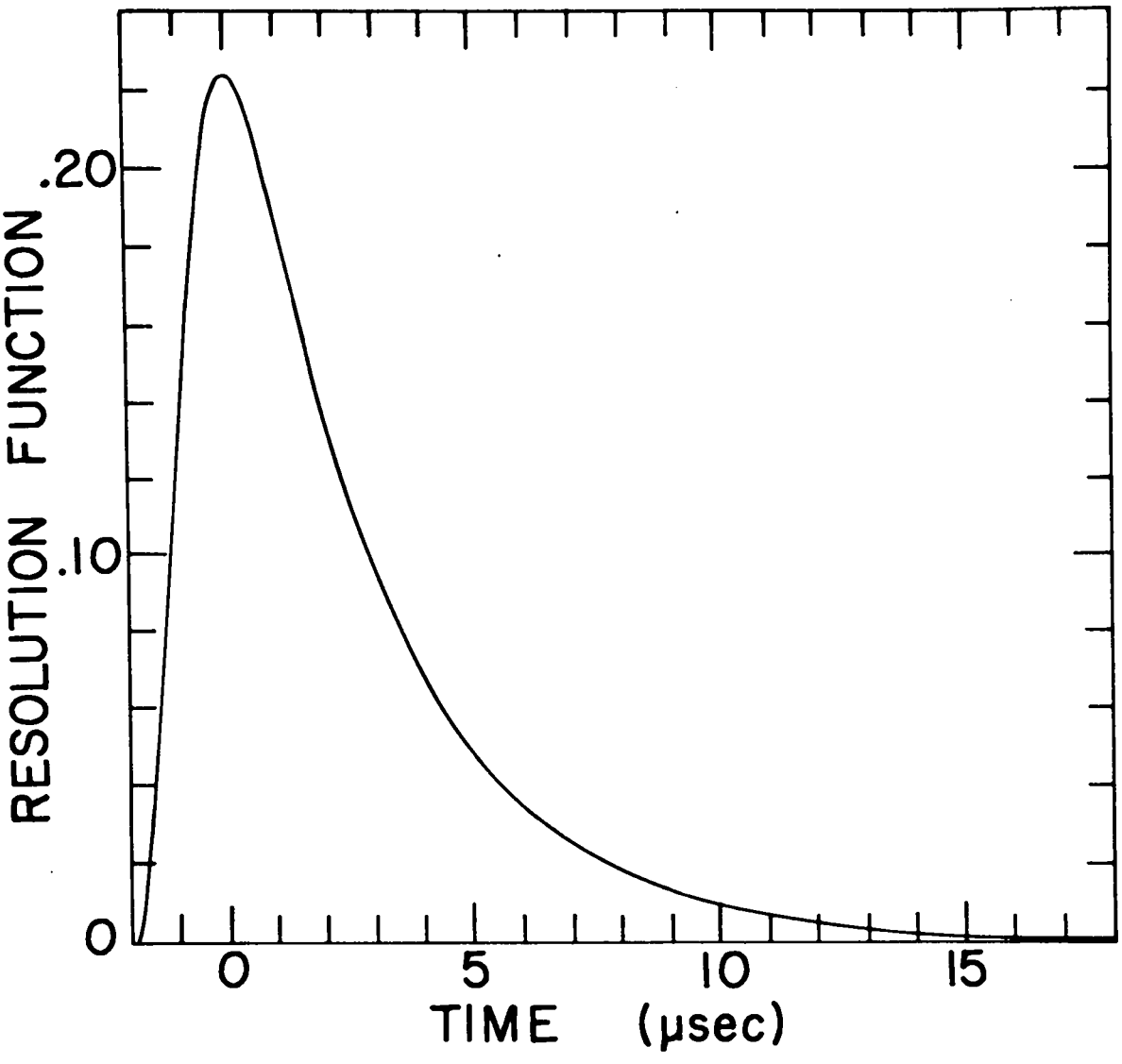

Fig. 17. The resolution function with which the computed cross sections were convoluted.

by neutron capture will have J^{π} of 2^+ or 3^+. A fission threshold appears to lie about 1.4 MeV below the energy of the ^{234}U compound nucleus,[28] and a second fission threshold falls about 0.7 MeV higher. According to the scheme of Wheeler[29] as extended by Lynn,[10] the first threshold is most likely a 2^+ rotation built on the ^{234}U ground state configuration while the second is due to a one quantum gamma vibration (producing 2^+ states) with rotational energy (producing 3^+ states). Finally, near the neutron threshold energy a mixed state of one quantum shape deformation (octupole vibration) plus one quantum bending (2^+) with rotational energy (3^+) may occur. Thus, one would expect at least two open channels from the 2^+ and one from the 3^+ state. One additional partially, or fully, open channel may exist for both spins.

In fitting the fission data with the multilevel formalism three open channels were assumed. For the sake of simplicity, however, each resonance was permitted to have a fission width in only one channel. This, barring correlating quantum effects, is an invalid assumption, for if two channels of average fission widths $\langle\Gamma_1\rangle$ and $\langle\Gamma_2\rangle$ are open in a given spin state the probability of a resonance having the fraction R or less of its fission width Γ_f in either channel is given by the integral of the product of two Porter-Thomas distributions[30] of one degree of freedom

$$P(R) = 1 - \frac{1}{2\pi}\int_0^{\infty} dy \int_a^b \frac{e^{-\frac{1}{2}(x+y)}}{\sqrt{xy}}\, dx$$

where $x = \Gamma_2/\langle\Gamma_2\rangle$,

$y = \Gamma_1/\langle\Gamma_1\rangle$,

$a = y\,\frac{R}{1-R}\,\frac{\langle\Gamma_1\rangle}{\langle\Gamma_2\rangle}$,

$$b = y \frac{1-R}{R} \frac{\langle \Gamma_1 \rangle}{\langle \Gamma_2 \rangle} \quad \text{and}$$

R can take all values between 0 and $\frac{1}{2}$.

Table 4 lists the probabilities for R and various ratios, G, of $\langle \Gamma_1 \rangle / \langle \Gamma_2 \rangle$.

TABLE 4

The Probability of Mixed Resonances - 2 Channel Case

G	P(1/10)	P(1/5)	P(1/3)	P(1/2)
0.2	0.51	0.68	0.84	1.0
0.5	0.44	0.62	0.80	1.0
1.0	0.43	0.60	0.79	1.0

Resonances with R = 1/5 or less would be very difficult to recognize as multi-channel. Since the 2^+ state is expected to have at least two open channels, 30-40% of the 2^+ resonances violate the assumption used in the fit. The situation may be better for the 3^+ states.

The values for Γ_γ selected in the fits were somewhat arbitrarily chosen. The 45 meV, used for the single level fit, was chosen to permit a direct comparison to Nifenecker's results.[9] The values for the multilevel study, 40 meV for channels of smaller $\langle \Gamma_f \rangle$ and 65 meV for the widest $\langle \Gamma_f \rangle$, were guided by Moore's[22] study of a few low energy resonances in ^{233}U.

The fits to the fission data are shown in Figs. 12 and 13 for the single and multilevel, respectively.

The fit to the $(\sigma_f + \sigma_\gamma)$ data is shown only for the multilevel analysis (Fig. 14) and the results of α for both

fits in Figs. 15 and 16. As was stated earlier, the fits were made to the fission data; when the fit was completed the parameters were used to derive the curves for $(\sigma_f + \sigma_\gamma)$ (Fig. 14) and α (Figs. 15 and 16). It is apparent that while the fit to the fission data is quite good, the single level fit to the α shows agreement only in the limited region 32-36 eV. The results of the multilevel analysis, on the other hand, show fair agreement in shape up to 50 eV but at higher energies appear to suffer from missed levels. The weak fluctuations of Γ_γ from resonance to resonance, not considered here, could also improve the α fits but are not expected to cause large changes.

As other investigators have stated, the single level α comparison graphically demonstrates that the single level parameters can be used to reproduce the cross sections upon which the fit is based but do not describe the physical situation. The multilevel formalism, on the other hand, shows promise and should be studied in more detail before being accepted or rejected as a proper tool for classifying resonance parameters.

The parameters obtained from the fits are listed in Tables 5 and 6. Sixty-eight and fifty-four levels were required for the single level and multilevel fits, respectively. The reduced number for the multilevel is a direct result of the added parameter (the sign of the reduced width).

Plots of the level density, partial sum of reduced neutron width, reduced neutron width, fission width, and level spacing distributions are shown in Figs. 18 and 19 for the single and multilevel parameters, respectively. Averages of the spacings and widths are listed on the plots. The strength function $S = 2g\Gamma_n^o/\text{"D"}$ listed in (a) of each figure was determined from the slope of the least squares

TABLE 5

Single Level Resonance Parameters

Energy (eV)	$2g\Gamma_n^o$ (mV)	Γ_f (mV)	Γ_γ (mV)	Energy (eV)	$2g\Gamma_n^o$ (mV)	Γ_f (mV)	Γ_γ (mV)
20.58	0.38	360.	45.	39.32	0.056	250.	45.
21.88	0.53	200.		39.56	0.055	250.	
22.36	1.51	350.		39.89	0.145	600.	
22.96	0.18	450.		40.49	0.175	650.	
23.78	0.22	390.		41.06	0.091	190.	
24.26	0.105	530.		41.75	0.009	150.	
24.64	0.01	200.		42.16	0.035	350.	
25.27	0.30	260.		42.66	0.19	140.	
25.75	0.10	340.		43.53	0.093	240.	
26.08	0.05	200.		44.58	0.086	660.	
26.30	0.035	100.		45.38	0.006	180.	
26.65	0.17	300.		46.16	0.105	150.	
27.05	0.015	200.		46.71	0.01	200.	
27.74	0.135	800.		47.05	0.075	400.	
28.00	0.007	130.		47.36	0.13	220.	
28.32	0.105	250.		48.76	0.445	175.	
28.85	0.135	320.		49.30	0.050	200.	
29.12	0.338	290.		50.48	0.184	900.	
29.59	0.073	150.		51.23	0.021	260.	
30.30	0.02	130.		52.06	0.016	300.	
30.73	0.215	260.		53.17	0.19	290.	
31.35	0.10	230.		53.54	0.055	300.	
31.66	0.075	200.		54.15	0.30	400.	
32.04	0.30	170.		54.89	0.33	320.	
33.11	0.27	750.		55.81	0.23	500.	
33.67	0.11	500.		56.18	0.20	300.	
34.06	0.155	480.		56.58	0.34	450.	
34.55	0.37	550.		57.55	0.74	900.	
35.27	0.114	450.		58.54	0.23	350.	
35.62	0.024	300.		59.35	0.009	300.	
35.96	0.14	750.		60.38	0.045	500.	
36.59	0.20	110.		61.07	0.08	280.	
37.51	0.21	380.		61.50	0.36	400.	
39.08	0.055	200.		62.72	0.29	165.	

TABLE 6

Multilevel Resonance Parameters

Energy (eV)	$2g\Gamma_n^o$ (mV)	Γ_f for the Three Channels (mV)			Γ_γ (mV)
20.535	0.32		+320		40.
21.885	0.49	+190.			40.
22.33	1.34		-355.		40.
22.94	0.61			+950.	65
23.61	0.185		-540.		40
25.245	0.25			+220	65
25.84	0.013	-40.			40.
26.3	0.115		+550.		40.
26.63	0.19	-330.			40.
27.28	0.0074		+250.		40.
27.69	0.14			-725.	65.
28.35	0.09	+200.			40.
29.11	0.5		+420.		40.
29.55	0.105	+250.			40.
30.0	0.005	+10.			40.
30.41	0.045	-200.			40.
30.72	0.235		+260		40.
31.1	0.025	+20.			40.
31.3	0.128			-440	65.
32.06	0.27	-160.			40.
32.94	0.125		+620.		40.
34.14	0.29			+850	65.
34.64	0.37		-450.		40.
35.43	0.51			+1500	65.
36.615	0.20	+120.			40.
37.505	0.198		+365		40.
39.18	0.08		-350.		40.
39.39	0.22			+660.	65.
40.83	0.126			-740	65.
41.03	0.115	+200.			40.

TABLE 6 (continued)

Energy (eV)	$2g\Gamma_n^o$ (mV)	Γ_f for the Three Channels (mV)		Γ_γ (mV)
41.90	0.034	-460.		40.
42.69	0.21	-170.		40.
43.495	0.104	+240.		40.
44.69	0.102	-690.		40.
45.50	0.011	-72.		40.
46.16	0.11	-150.		40.
47.36	0.20	+385.		40.
48.79	0.49	+90.		40.
49.29	0.085	-190.		40.
50.48	0.23		+1000.	65.
51.25	0.036	+390.		40.
51.98	0.036	-400.		40.
52.5	0.017	-240.		40.
53.16	0.29		+400.	65.
54.15	0.285	+330.		
54.83	0.275	-260.		
56.16	0.305	+500.		
56.56	0.39	-380.		
57.60	0.74		-800	65.
58.59	0.21	+290.		40.
59.10	0.01	-110.		40.
60.08	0.01	+20.		40.
61.62	0.45		+510	65.
62.71	0.33	-130.		40.

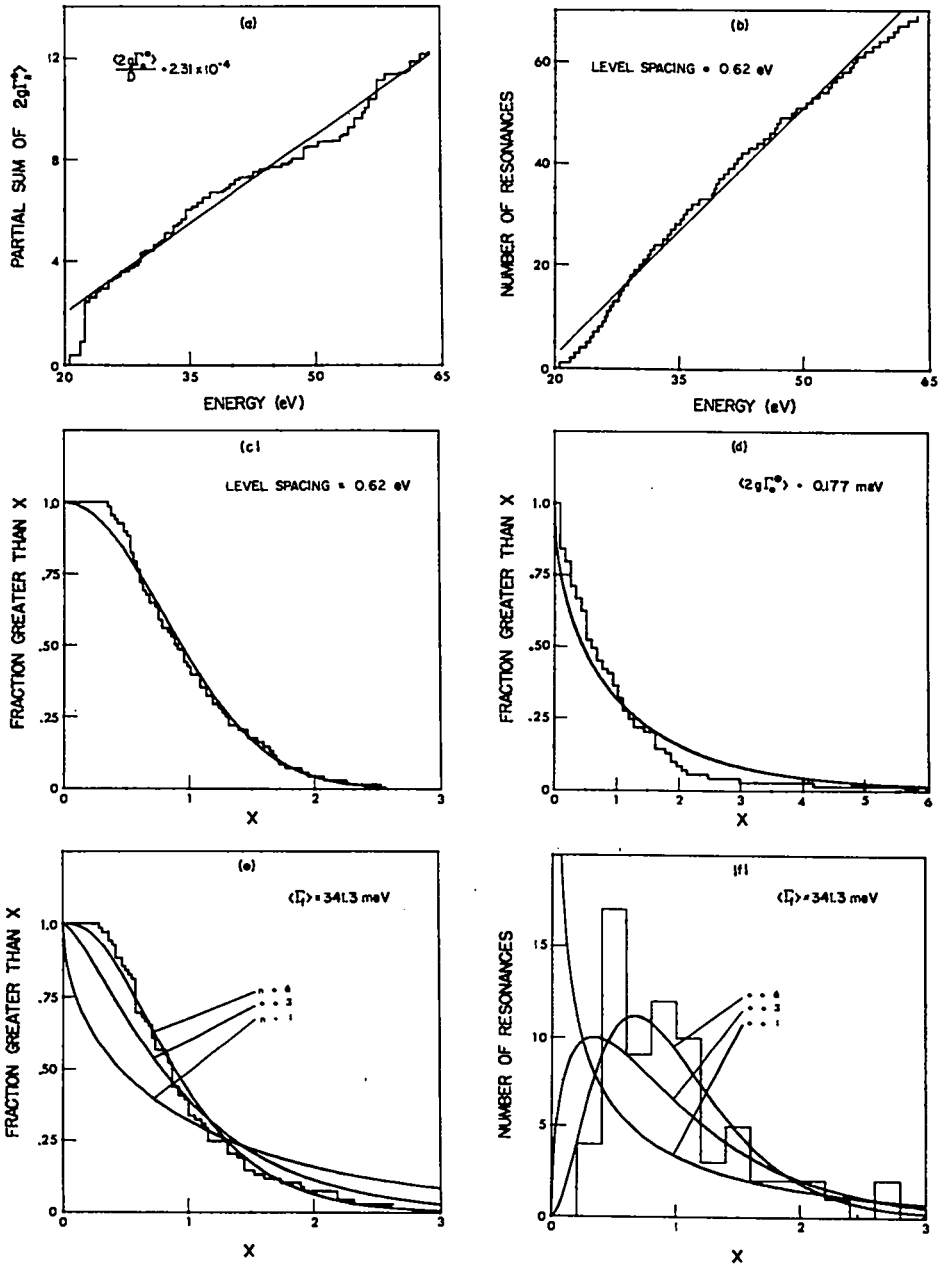

Fig. 18. Single level resonance - parameter study.

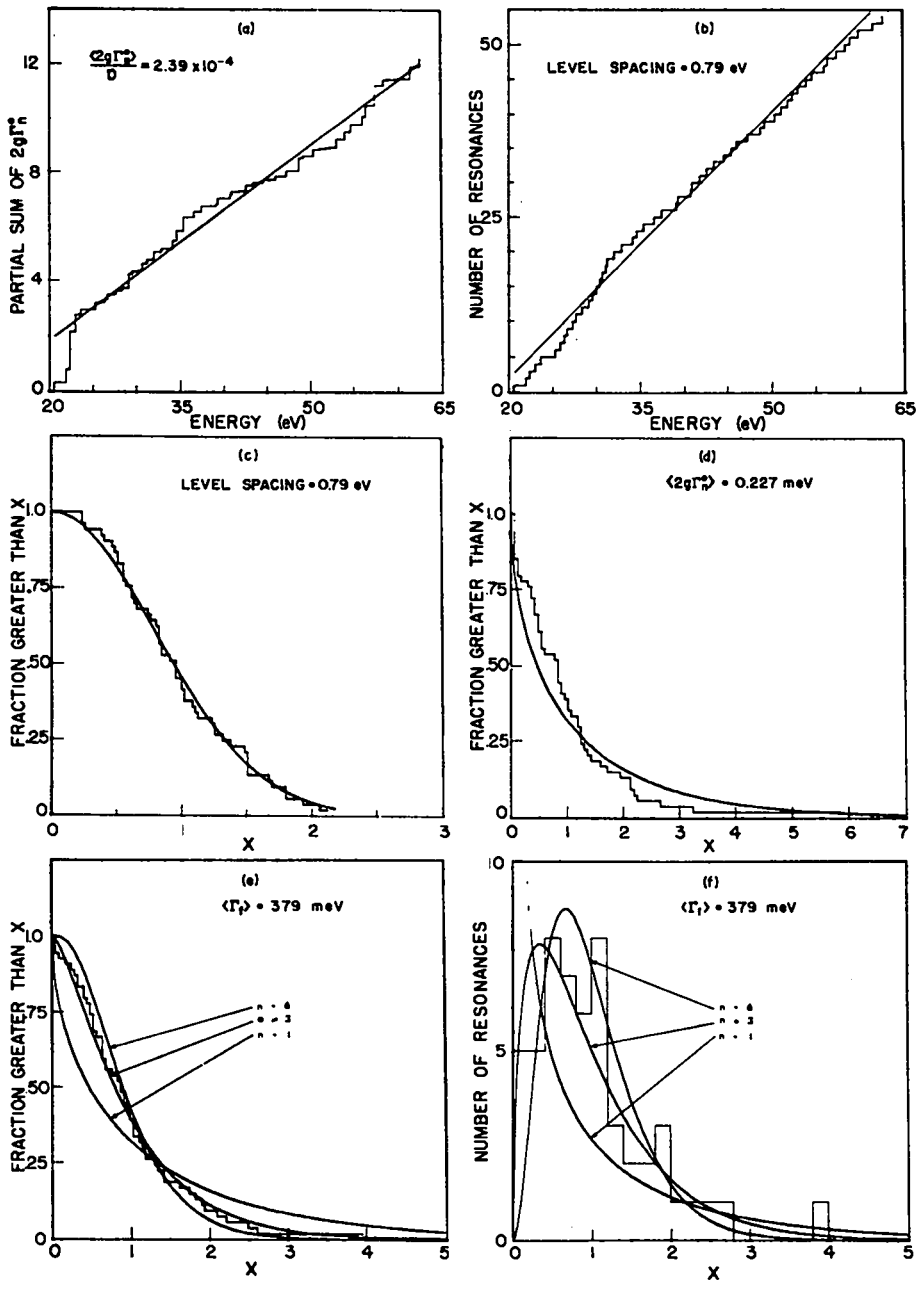

Fig. 19. Multilevel resonance - parameter study.

fit to the data ("D" is the average spacing of all levels). Both the single level value 2.31×10^{-4} and multilevel value 2.39×10^{-4} compare favorably with that quoted by Nifenecker,[9] 2.09×10^{-4}. Assuming that only levels with small Γ_n^o have been left out of the fit, the quoted values of S should not significantly change (see study in Sec. IV). A renormalization of the fission cross section would, however, change the Γ_n^o's, and therefore, S in the same proportion.

The slight curvature of the level spacing plot--(b) of Figs. 18 and 19--suggests that a few levels have been overlooked above 50 eV in both fits. This is also supported by the difficulties in the α fits in that region. The quoted level spacing was derived from the least squares line drawn through the data, and missed levels would seriously alter these values.

The level spacing integral histogram, Figs. 18 and 19 (c), fits the Wigner[31] spacing distribution for one family

$$P(x)dx = \frac{\pi x}{2} e^{-\pi x^2/4} dx$$

where x is the ratio of level spacing to average spacing [integral form is shown as the smooth curve in Figs. 18 and 19 (c)]. The distribution is the result of two families (2^+ and 3^+ states) and this agreement is, no doubt, a result of closely spaced levels being combined as one.

The integral form of the reduced neutron width histogram is shown in Figs. 18 and 19 (d). The smooth curve is the integral form of the Porter-Thomas[30] width distribution for one degree of freedom

$$P(x)dx = \frac{1}{\sqrt{2\pi x}} e^{-\frac{1}{2}x} dx, \quad x = \frac{\Gamma_n^o}{\langle \Gamma_n^o \rangle} .$$

The disagreement is again the result of missing the very narrow levels. The value 0.177 meV for $\langle 2g\Gamma_n^o \rangle$ obtained from the single level compares favorably with the value 0.169 meV found by Nifenecker.[9] The 0.227 meV from the multilevel is considerably larger--as expected.

The fission width distribution should not be as affected by missing weak levels, i.e., small Γ_n^o; it will, however, be distorted when multi-resonance peaks are combined as one. The values 341 meV and 379 meV for $\langle \Gamma_f \rangle$ from the single and multilevel fits, respectively, compare with the value 389 meV found by Nifenecker.[9] The integral and differential fission width histograms are shown as (e) and (f) of Figs. 18 and 19. Porter-Thomas distributions for 1, 3, and 6 open channels are also displayed on the histograms. The best fit for the multilevel plot Fig. 19 appears to be about 3.5, while that for the single level exceeds 6. The total number of open channels calculated from the equation[32]

$$\nu = \frac{2\langle \Gamma_f \rangle^2}{\langle \Gamma_f^2 \rangle - \langle \Gamma_f^2 \rangle}$$

gives:

$\nu = 6.68$ single level

$\nu = 3.62$ multilevel.

The total channel openness, calculated from the eq.

$$\nu = 2\pi\langle \Gamma_f \rangle / \text{"D"}$$

gives:

$\nu = 3.46$ single level

$\nu = 3.01$ multilevel.

A detailed look at the multilevel fission and α fit shows that the major discrepancy occurs at a high cross section region around 56 eV which was fitted with several broad levels. This no doubt is incorrect, and at least two to three of the peaks have led into the trap discussed above (i.e., the effect of two or more resonances appearing as one level).

The possibility of a level being composed of partial fission widths from several channels does not seem to have led to difficulty in the fit, although the region 45-50 eV may show this effect. Since as many as ten levels should have shown this, its apparent lack may be the result of quantum or correlation effects. Assignment of spins is impossible although it is plausible to assume the widest group (Γ_{f_3} in Table 5) to be 2^+ levels.

A remeasurement of the ^{233}U cross sections with better energy resolution may improve the interpretation. Certainly the precise simultaneous measurement of total, or capture, and fission cross sections is needed for a proper classification of resonance parameters of fission isotopes. The methods used in this investigation (i.e., a very intense single-pulsed source), lend themselves particularly well to such simultaneous measurements.

IV. MULTILEVEL CROSS SECTION INTERPRETATION

In view of questions raised on the validity, and therefore desirability, of fitting fission data with the currently available multilevel equations, this section is devoted to the physical results which one might derive from the Reich-Moore[22] formalism.

Lynn[10] demonstrated clearly the difficulties associated with interpreting the cross section resulting from two levels of different widths lying quite close together. A similar study has been carried out here for both two and three levels, which indicates that the presence of close lying levels of a given spin may be determined with the aid of α data. For the two level case, resonances were choosen with parameters, Γ_γ = 40 meV, Γ_{f1} = 60 meV, Γ_{f2} = 300 meV, Γ_{n1}^o = 0.09 meV, and Γ_{n2}^o = 0.2 meV. The energy of the second resonance was held fixed at 30 eV while the first resonance was moved past it. The separations were chosen at 2, 1, 0.5, 0.2, 0.1, 0, and -0.2 eV. The results of both the fission cross section and the capture to fission ratio, α, are shown in Fig. 20 (single level), Fig. 21 (multilevel with the signs of $\sqrt{\Gamma_n \Gamma_f}$ both positive) and Fig. 22 (multilevel with opposite signs on $\sqrt{\Gamma_n \Gamma_f}$). The small arrows shown on each figure mark the location of the narrow resonance; the position of the broad resonance is marked with a single broad arrow.

The curves have been Doppler-broadened assuming room temperature; resolution broadening was not performed. The variations in α are quite spectacular and leave little doubt

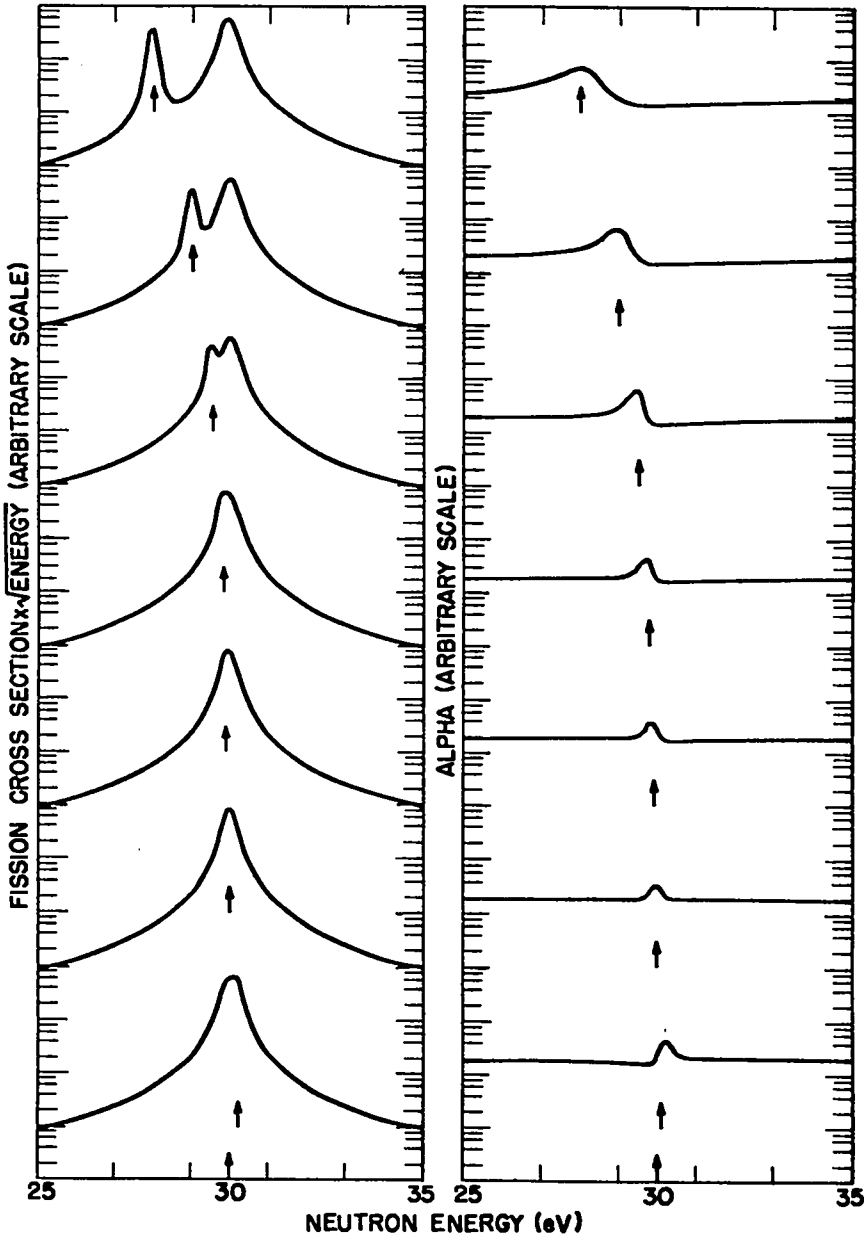

Fig. 20. Two resonance study showing $\sigma \cdot \sqrt{E}$ and α. The values were derived using the single level equation.

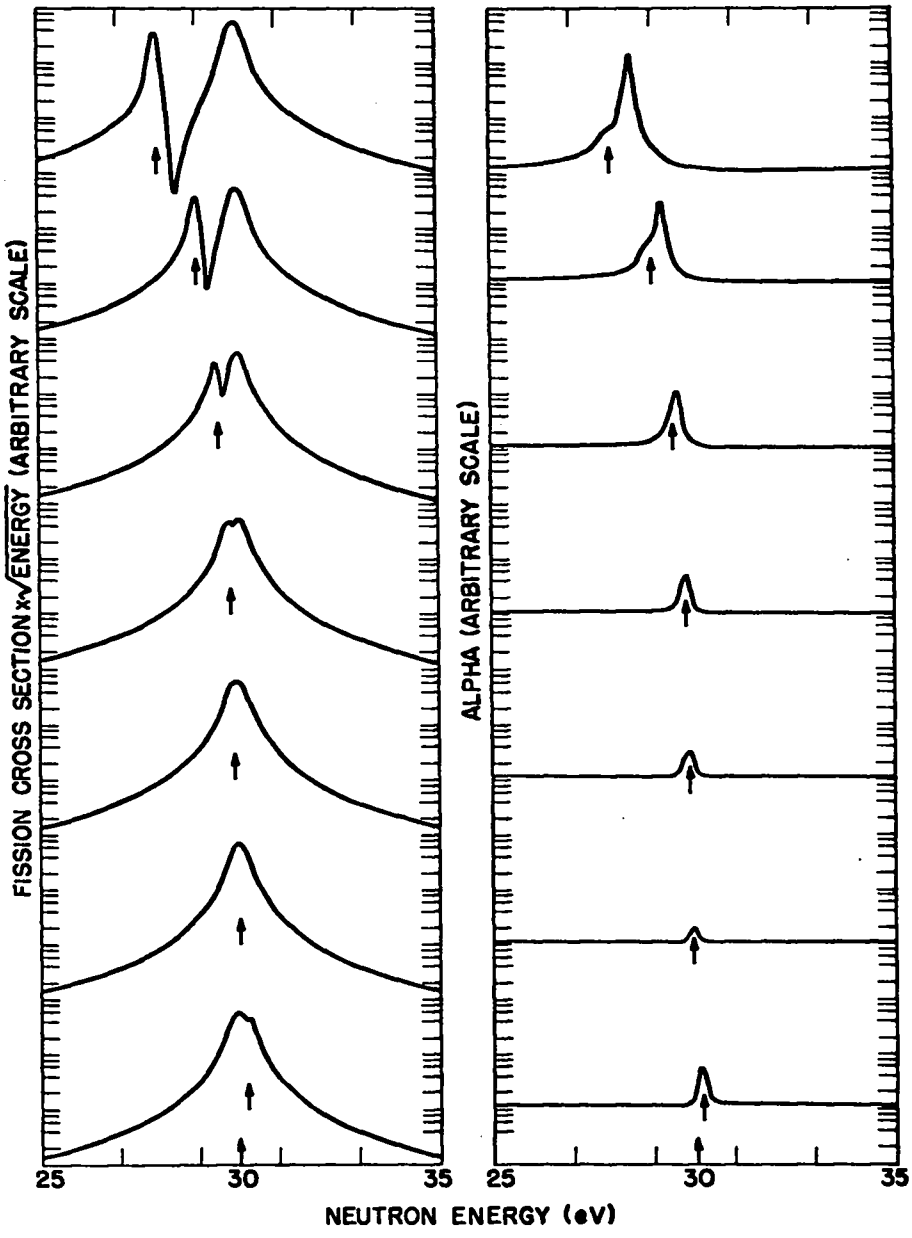

Fig. 21. Multilevel resonance study showing $\sigma \cdot \sqrt{E}$ and α. The sign of $\sqrt{\Gamma_n \Gamma_f}$ was the same for both resonances.

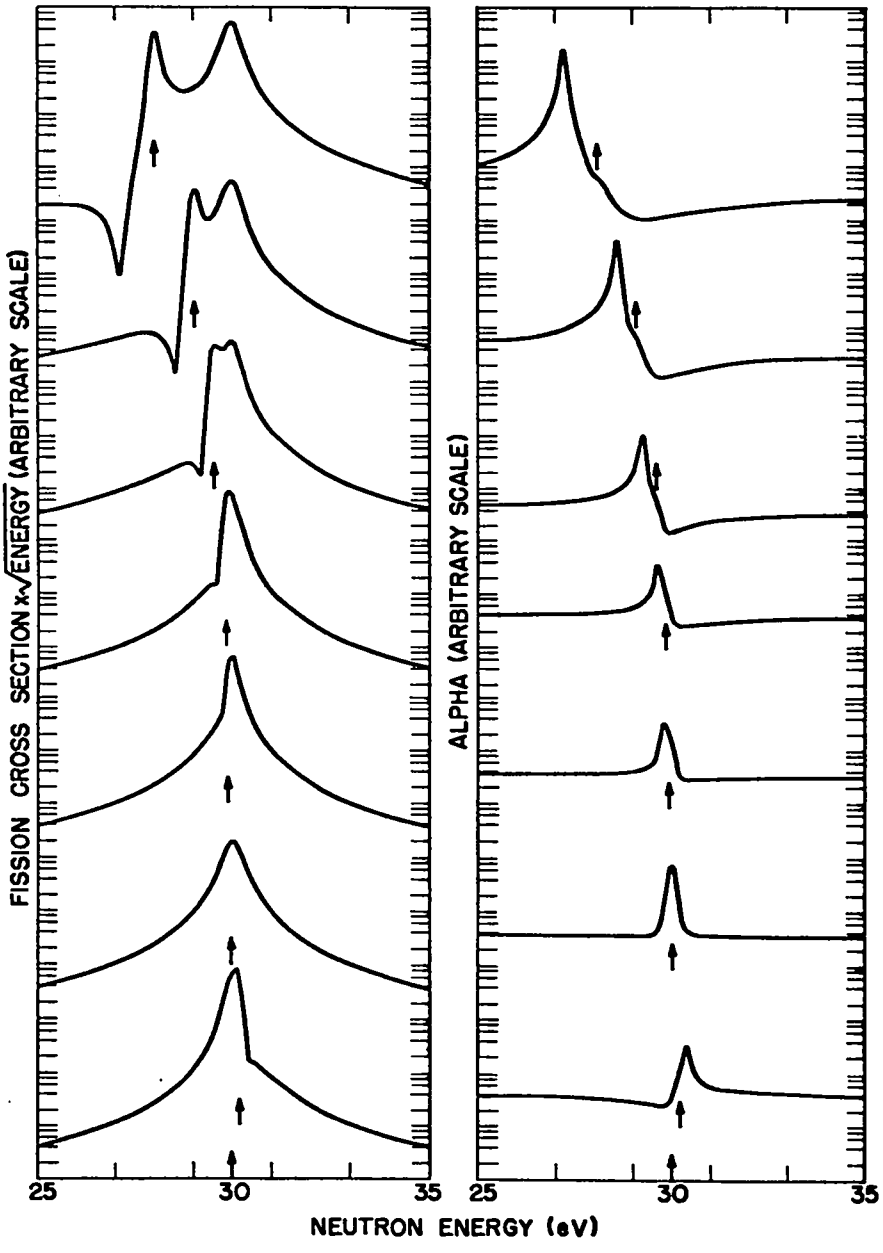

Fig. 22. Multilevel resonance study showing $\sigma \cdot \sqrt{E}$ and α. Opposing signs were given to $\sqrt{\Gamma_n \Gamma_f}$ for each resonance.

in the position and relative sign of the two resonances, although in the case of near superposition the levels always appear as one. The value of α on the right hand edge of each graph is approximately: 0.2 (Fig. 20), 0.1 (Fig. 21), ~.3-.4 (Fig. 22). The single level case describes the situation for levels in different spin states; even here, with near superposition (a much more probable situation than for the resonances from the same spin state) the α data clearly indicate the presence of two levels. This variation of course becomes weaker in the presence of additional levels or as the ratio Γ_γ/Γ_f becomes more nearly the same for the two levels.

The three level case with Doppler broadening is shown in Fig. 23. The parameters used were:

TABLE 7

Parameters for 3 Level Case

Resonance	E (eV)	Γ_n^o (meV)	Γ_f (meV)	Γ_γ (meV)
1	29.2	0.230	340.	45.
2	30.0	0.230	340.	45.
3	30.8	0.230	340.	45.

Five cases were considered including the single level (lower curves) and all possible relative signs of the reduced widths (see symbols shown on each of the upper four curves) for the multilevel cases.

Again, all cases except the single level (an unlikely physical situation for one isotope) are unambiguously determined by combining the α data with the fission results.

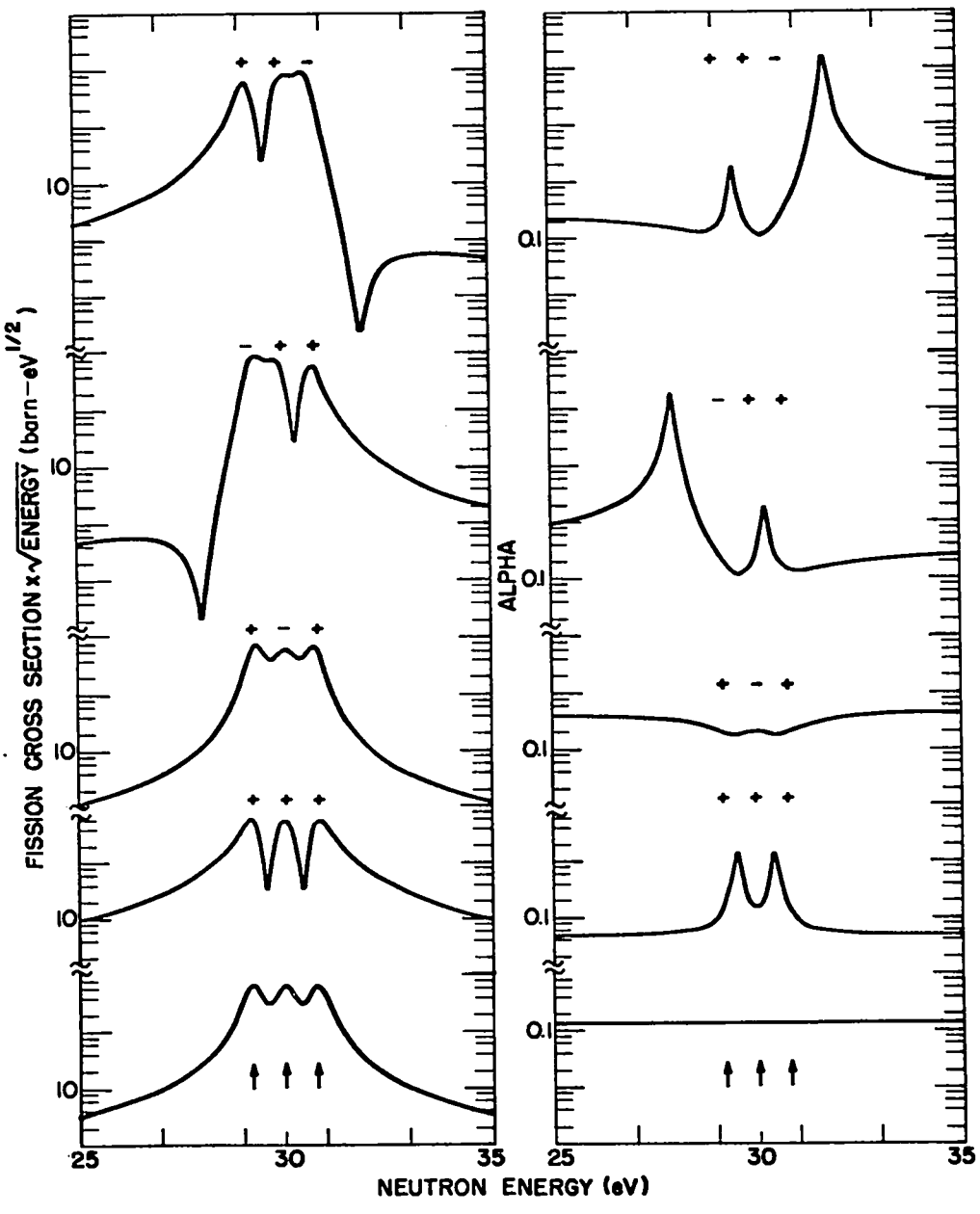

Fig. 23. Three resonance study showing $\sigma \cdot \sqrt{E}$ and α for the single level equation (lower curves) and the multilevel equation. The relative sign for $\sqrt{\Gamma_n \Gamma_f}$ is shown above each curve.

The rather dramatic change in the average value of α for each curve should also be noted. These results strongly suggest that the simultaneous measurement of fission and capture cross sections could be uniquely interpreted by R matrix formalism in the simple case of one open channel per spin state.

To check this result in a realistic situation a set of resonance parameters, randomly generated using the procedure discussed by Moore,[33] were used to compute a mock fission cross section and α. (see Figs. 24 and 25). The parameters chosen were based on spacings and averages found in ^{233}U according to the Wigner spacing equation and Porter-Thomas width distribution. Higher order correlations were not taken into account. Two spin states, each with two open channels, were assumed and the ratio of average level spacing was chosen to vary inversely as $2J + 1$. The fission width of the second channel was assumed to be half that of the first for both states. The $\langle \Gamma_n^o \rangle$ selected was not corrected for missed levels and thus the average cross section is larger than expected for ^{233}U. σ_f (Fig. 24) and α (Fig. 25) are qualitatively similar to that of ^{233}U except near 40 eV. Sixty two levels fall in the range 20-63 eV (see arrows). Based on the number of bumps (which one would assume to be due to a resonance) in the mock and fission data, and the number of resonances required to fit the ^{233}U data, one might expect to use 48 resonances to fit the mock data (about 3/4 of the true number).

After examining the results, thirteen of the narrow Γ_n^o resonances which did not appear to affect the data strongly were removed (these are noted with o's in Figs. 24 and 25) and the remaining resonances were used to compute a new mock cross section. The results of $\sigma_f \cdot \sqrt{E}$ and α are

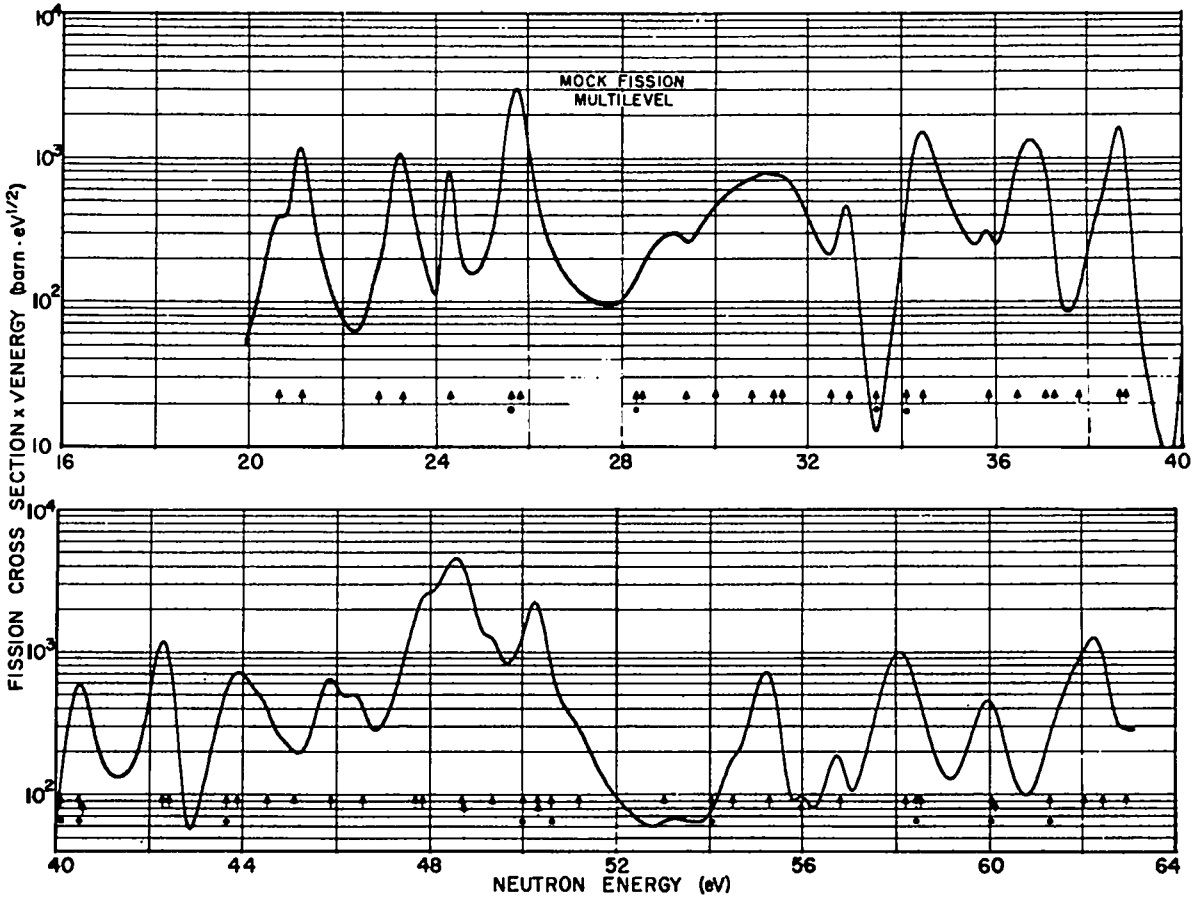

Fig. 24. The mock fission cross section times $\sqrt{E}$ as determined from the multilevel equation. Arrows mark the location of resonances.

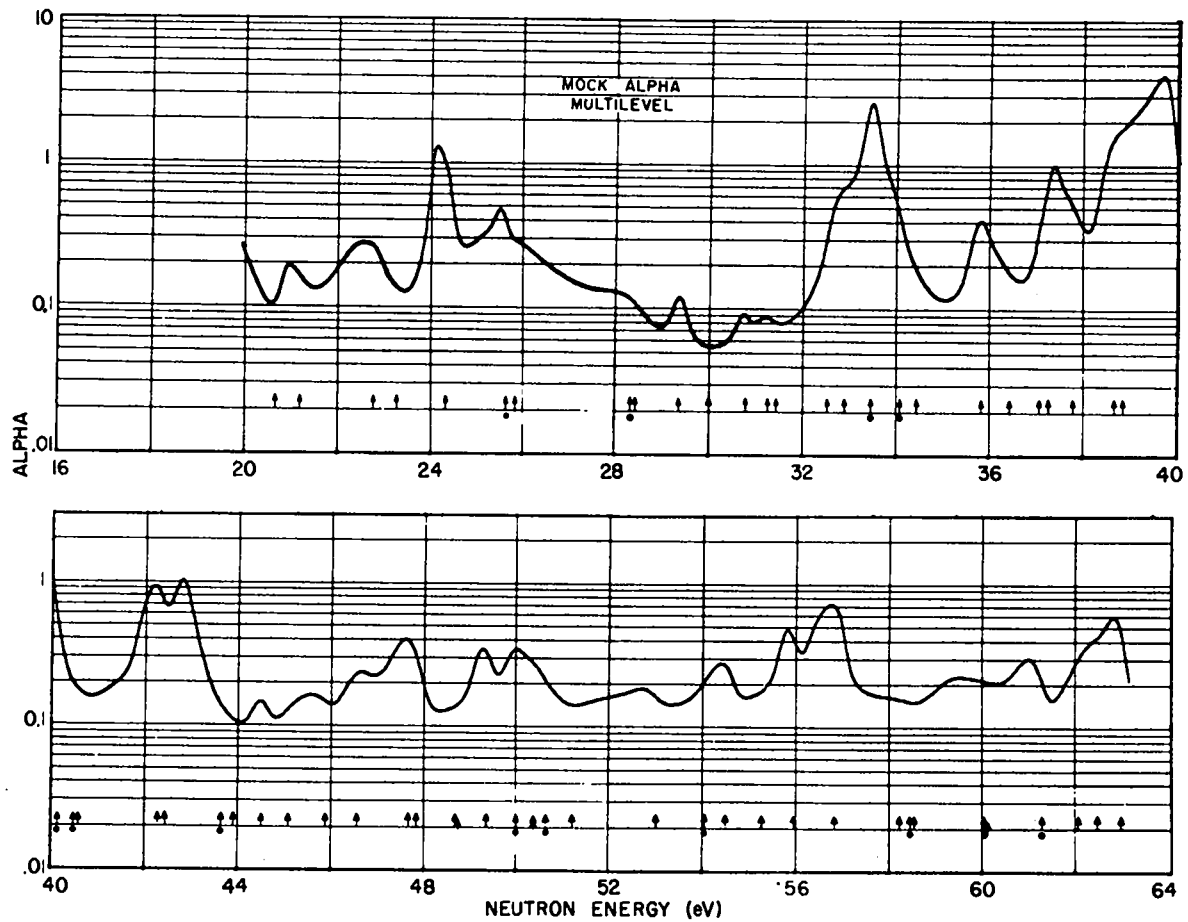

Fig. 25. The mock α as determined from the multilevel equation. Arrows mark the location of resonances.

shown in Figs. 26 and 27 (x's mark the location of the omitted resonances) and appear very much like the original run; if these were experimental data, a significant variation between the "fit" (Fig. 26) and the "data" (Fig. 24) could be noted at only about two of the omitted resonances. The availability of precise α data would allow a few more missing levels to be located, but it does not appear possible to locate the entire set. It is quite likely that the multi-resonance peaks (e.g., 42 and 48.5 eV) could be fitted well with single resonances considering only σ_f data. In fact it is not apparent from the α data that these are multi-resonance peaks. An independent measurement for α might resolve the issue.

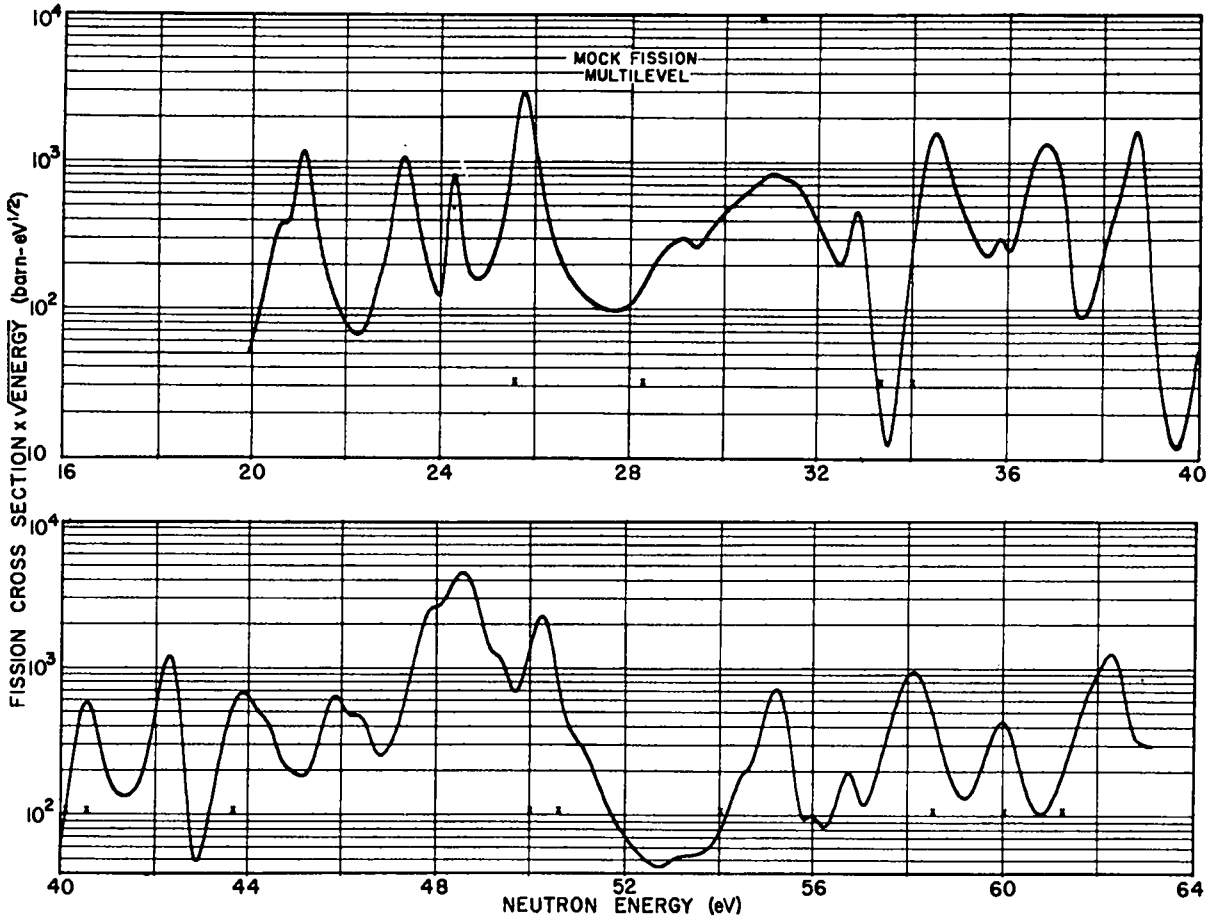

Fig. 26. The revised mock fission cross section times $\sqrt{E}$. X's mark the location of omitted resonances. All other resonances shown in Fig. 24 were included.

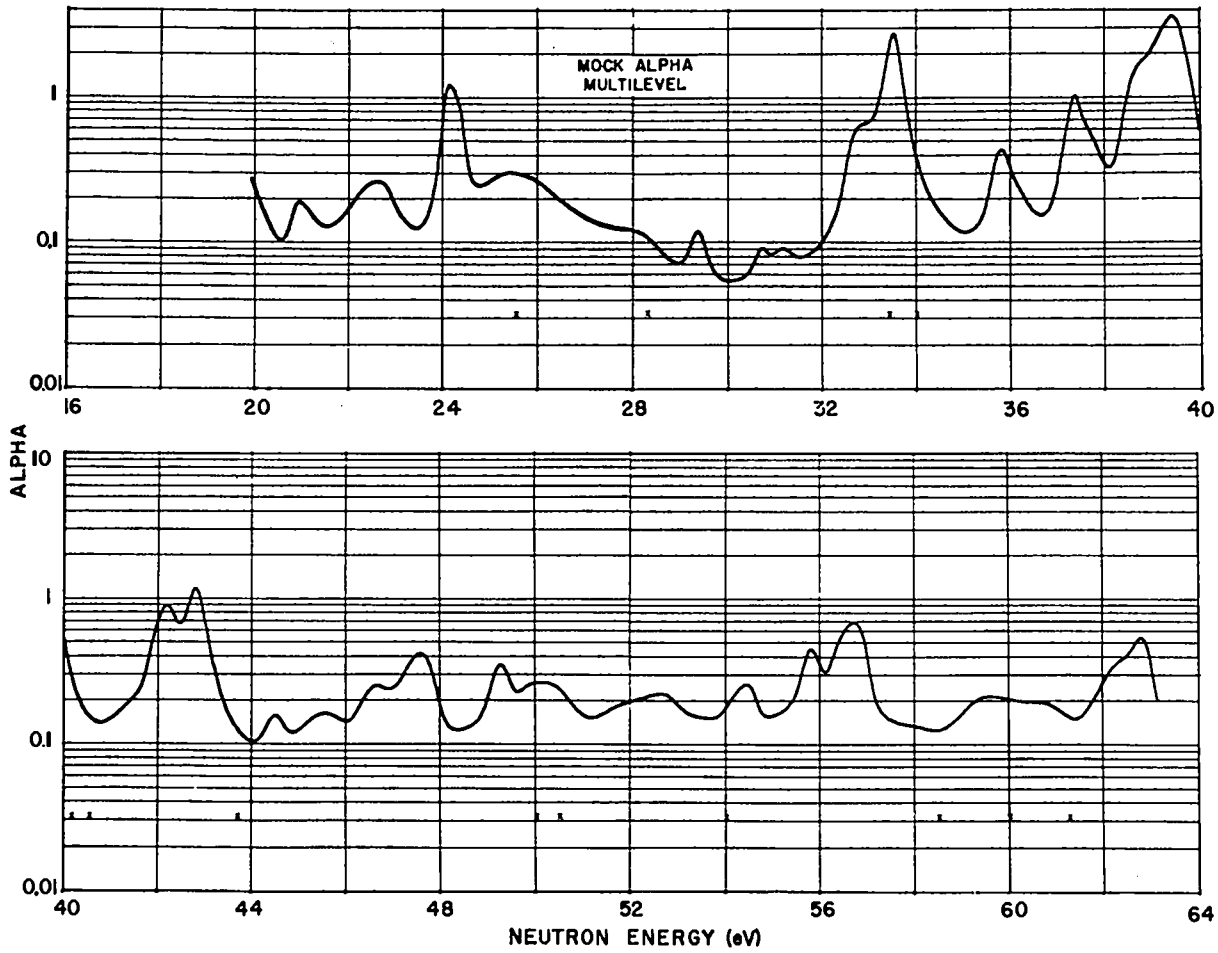

Fig. 27. The revised mock α using the resonances included in Fig. 26.

V. SUMMARY

It is hopeless to expect a valid physical interpretation of fission data from a single level fit. It is also doubtful, in view of the mock data results, that a multilevel fit yields a unique interpretation.

The single level and multilevel parameters listed in Tables 5 and 6 will recreate the fission cross section for ^{233}U as measured on Petrel. Because of the many artificial resonances introduced in the single level fit it should be used with caution in reactor studies.

The validity of the resonance parameters derived from the multilevel fit is somewhat uncertain; it is, however, the conclusion of this author (based on the mock fission "data") that as many as 25-30% of all resonances have been missed, but that almost all of these levels are quite weak. Also, because of the fitting of multi-resonance peaks with a single resonance as many as 10% of the resonance parameters are completely incorrect. With high precision data for both fission and α the situation could be greatly improved.

Because the strength function is relatively unaffected by missing-weak levels (e.g., the computed value of S for the two sets of mock data differed by only 3%) the values listed for the Petrel data are as accurate as the data itself within the statistical spread expected for the number of levels involved.

The number of fission channels determined from the multilevel fit agree well with that suggested by Lynn[10] and Wheeler.[29]

Finally, this few level study suggests that the difficulty discussed by Lynn[10] may be largely overcome for fissionable nuclei with the simultaneous fitting of fission and capture data using the R matrix formalism.

LIST OF REFERENCES

1. B. C. Diven in: Proceedings of the International Conference on the Study of Nuclear Structure with Neutrons, eds: M. Nève de Mévergnies, P. Van Assche, and J. Vervier. (North Holland Publishing Co. Amsterdam, Holland) p. 441.

2-6 CONF-660303 (March 1966), Obtainable from the Federal Clearinghouse for Scientific and Technical Information, National Bureau of Standards, U. S. Department of Commerce, Springfield, Virginia 22151.

2. D. W. Bergen, M. G. Silbert, and R. C. Perisho, p. 895.
3. Wilbur K. Brown, D. W. Bergen, and J. D. Cramer, p. 971.
4. Edward R. Shunk, W. K. Brown, and R. LaBauve, p. 979.
5. D. H. Byers, B. C. Diven, and Myron G. Silbert, p. 903.
6. O. D. Simpson, Rex G. Fluharty, M. S. Moore, N. H. Marshall, B. C. Diven, and Arthur Hemmendinger, p. 910.

7. P. A. Seeger, A. Hemmendinger, and B. C. Diven, Fission Cross Sections of ^{241}Am and ^{242}Am. (Submitted to Nuclear Physics).
8. Unpublished staff report LA-3586 Fission Cross Sections from Petrel. Sept. 1966. Available as Ref. 2.
9. H. Nifenecker and G. Perrin in Proceedings of the Symposium on Physics and Chemistry of Fission (International Atomic Energy Agency, Vienna 1965). p. 245.
10. J. E. Lynn, p. 125, Ref. 1.
11. M. C. Moxon and E. R. Rae, Nuclear Instruments and Methods 24, 445, (1963).
12. B. C. Diven, private communication (1966).

13. S. Schwarz, L. G. Strömberg, and A. Bergstrom, Nuclear Physics 63, 593 (1965).
14. D. H. Byers, private communication, (1966).
15. M. S. Moore, L. G. Miller, and O. D. Simpson, Phys. Rev. 118, 714 (1960).
16. Nifenecker, D. Pays, and J. Fagot, Journal De Physique 24, 254 (1963).
17. N. J. Pattenden and J. A. Harvey, Nuclear Science and Engineering: 17, 404 (1963).
18. R. D. Albert, Phys. Rev. 142, 778 (1966).
19. G. D. James, Proceedings of the International Conference on Fast Critical Experiments and Their Analysis (October 1966), (to be published as an Argonne National Laboratory report).
20. J. L. Perkin, P. H. White, P. Fieldhouse, E. J. Axton, P. Cross, and J. C. Robertson, Journal of Nuclear Energy A/B 19, 423 (1965).
21. John R. Stehn, Murray D. Goldberg, Renate Wiener-Chasman, Said F. Mughabghab, Benjamin A. Magurno, and Victoria M. May. Neutron Cross Sections Z = 88 to 98, BNL 325-III Suppl. No. 2 (Associated Universities, Inc. 1965).
22. M. S. Moore and C. W. Reich, Phys. Rev. 118, 718 (1960).
23. G. Breit and E. P. Wigner, Phys. Rev. 49, 519 (1936).
24. E. P. Wigner and L. Eisenbud, Phys. Rev. 72, 29 (1947).
25. C. W. Reich and M. S. Moore, Phys. Rev. 111, 929 (1958).
26. D. R. Harris, p. 823, Ref. 2.
27. A. Bohr, Proceedings of the International Conference on the Peaceful Uses of Atomic Energy, Geneva 2, 151 (1956).
28. J. A. Northrop, R. H. Stokes, and K. Boyer, Phys. Rev. 115, 1277 (1959).
29. John A. Wheeler in: Fast Neutron Physics Vol. II eds. J. L. Fowler and J. B. Marion (Interscience Publishers, New York, 1963), p. 2051.

30. C. E. Porter and R. G. Thomas, Phys. Rev. 104, 483 (1956).
31. E. P. Wigner, Proceedings of Conference on Neutron Physics by Time-of-Flight, ORNL-2309, available as Ref. 2, (1956) p. 59.
32. L. Wilets, Phys. Rev. Letters 9, 430 (1962).
33. M. S. Moore and O. D. Simpson, p. 840 Ref. 2.